NFIA and GATA3, critical regulators of embryonic articular cartilage differentiation

Pratik Narendra Pratap Singh[1, 5], Upendra Singh Yadav[1], Kimi Azad[1,2], Pooja Goswami[3], Veena Kinare[4], and Amitabha Bandyopadhyay[1†]

[1]Department of Biological Sciences and Bioengineering, Indian Institute of Technology, Kanpur, U.P. 208016, India.

[2]Current address: Kusuma School of Biological Sciences, Indian Institute of Technology Delhi, HauzKhas, New Delhi, Delhi 110016, India.

[3]Kalinga Institute of Industrial Technology, KIIT University, Bhubaneswar – 751024, Odisha, India.

[4]Department of Lifesciences, Sophia College for Women, Bhulabhai Desai Road, Mumbai - 400026, India.

[5]Current address: Department of Medical Oncology and Center for Functional Cancer Epigenetics, Dana-Farber Cancer Institute, Boston, MA 02215, USA.

[†]Corresponding author. E-mail: abandopa@iitk.ac.in (A.B.).

SUMMARY

During appendicular skeletal development, the bi-potential cartilage anlagen gives rise to transient cartilage, which is eventually replaced by bone, and articular cartilage which caps the ends of individual skeletal elements. While the molecular mechanism that regulates transient cartilage differentiation is relatively better understood, the mechanism of articular cartilage differentiation has only begun to be unraveled. Further, the molecules that coordinate articular and transient cartilage differentiation processes are very poorly understood. Here, we have characterized the regulatory roles of two transcription factors, NFIA and GATA3 in articular cartilage differentiation, maintenance and the coordinated differentiation of articular and transient cartilage. Both NFIA and GATA3 block hypertrophic differentiation. Our results suggest that NFIA is not sufficient but necessary for articular cartilage differentiation. On the other hand, while ectopic activation of GATA3 promotes articular cartilage differentiation, inhibition of GATA3 activity promotes transient cartilage differentiation at the expense of articular cartilage. Finally, we propose a novel transcriptional circuitry involved in embryonic articular cartilage differentiation, maintenance and its cross-talk with transient cartilage differentiation program.

INTRODUCTION

Vertebrate limb skeletogenesis starts as a Sox9 positive mesenchymal condensation which undergoes differentiation to become Col2a1 expressing cartilage. Concomitant to cartilage differentiation the anlagen is branched and segmented to give rise to most of the skeletal elements of the limb (Shubin, 1986; Bi et al., 1999). Barring the cartilage on either side of the plane of segmentation, the rest of the cartilage in these elements is gradually replaced by bone. The cartilage that is replaced by bone is referred to as transient cartilage while the cartilage that remains as cartilage is referred to as permanent or articular cartilage. The Col2a1 expressing chondrocytes present at the center of the cartilage primordium progressively differentiates into prehypertrophic chondrocytes, marked by *Ihh* expression, followed by maturation into ColX expressing hypertrophic chondrocytes (Karsenty and Wagner, 2002; Archer et al., 2003; Kronenberg, 2003; Pacifici et al., 2005). Recently, our group has demonstrated that the nascent cartilage cells are bi-potential in nature and can give rise to both transient and articular cartilage depending on their exposure to either BMP or Wnt signaling, respectively (Ray et al., 2015).

Interzone marks the site of future joint. Interzone is characterized morphologically by a region of densely packed flattened cells and molecularly by the presence of certain markers such as *Gdf5, Wnt9a, Atx*, and the absence of typical cartilage marker *collagen type II alpha1 (Col2a1)*. Interzone acts as a signaling center and is critical for joint morphogenesis (Holder, 1977; Archer et al., 2003; Pacifici et al., 2005). Wnt ligands, secreted from the interzone, activate Wnt/β-catenin signaling in the cells immediately adjacent to the interzone and is necessary for embryonic articular cartilage differentiation (Hartmann and Tabin, 2001; Guo

et al., 2004; Spater et al., 2006a; Spater et al., 2006b; Ray et al., 2015). Kan and Tabin discovered that transcription factor c-Jun is a critical transcriptional activator of Wnt ligands, namely Wnt9a and Wnt16 (Kan and Tabin, 2013). Thus, to date c-Jun, Wnt9a and β-catenin are the only molecules known to promote embryonic articular cartilage differentiation.

In addition, C-1-1, a *ch*-ERG variant, is the only reported joint specific transcription factor capable of inhibiting or blocking maturation of transient cartilage into hypertrophic chondrocytes. It should however be noted that even though C-1-1 can inhibit transient cartilage differentiation, it has not been reported to induce ectopic expression of articular cartilage markers other than Tenascin-C (Iwamoto et al., 2000; Iwamoto et al., 2001; Iwamoto et al., 2007).

As compared to other chondrocyte populations, our understanding of articular cartilage differentiation remains rudimentary despite tremendous progress in the past few decades. For instance, we do not have comprehensive knowledge of transcription factors that are critically important for articular cartilage differentiation neither do we know how articular cartilage evades hypertrophy and remains as permanent cartilage throughout (Karsenty and Wagner, 2002). These are critically important aspects as articular cartilage is the tissue which is affected, and suspected to undergo transient cartilage differentiation, in osteoarthritis, the most prevalent skeletal disease (Pitsillides and Beier, 2011).

Previously, we reported identification of a transcription factor *NFIA* to be expressed in chick embryonic articular cartilage (Singh et al., 2016). Here, we identified another transcription factor *GATA3* to be expressed in chick embryonic articular cartilage. We performed gain- and loss-of-function studies for both NFIA and GATA3. Loss-of-function of NFIA resulted in the reduction of the interzone region while that of GATA3 abrogated articular cartilage differentiation. On the other hand, gain-of-function of both these molecules blocked

hypertrophic cartilage differentiation but only GATA3 can induce ectopic expression of several articular cartilage markers. However, our results suggest that GATA3 needs to act in collaboration with other transcription factors for proper articular cartilage differentiation.

RESULTS

Knockdown of NFIA results in reduced interzone domain

In a previously conducted screen, we identified the transcription factor *NFIA* to be expressed in the outer chondrogenous layers (OCL) of developing chicken articular cartilage from HH28 to HH38 (Singh et al., 2016). In order to investigate the necessity of NFIA in articular cartilage differentiation, we downregulated the endogenous NFIA expression utilizing a well characterized RCAS based shRNAi (cNFIA-RNAi) against chick *NFIA*. The specificity and efficacy of this construct in knocking down endogenous chick *NFIA* has been reported previously (Deneen et al., 2006). Embryonic chick limb buds were infected at HH14 with RCAS virus particles expressing cNFIA-RNAi and were harvested at HH36 (supplementary material Fig.S1, also refer to Experimental Procedures). Knockdown of NFIA resulted in micromelia of the infected limbs (supplementary material Fig. S2C,D) compared to the uninfected contralateral limbs (supplementary material Fig. S2A,B). Skeletal prep analysis of cNFIA-RNAi infected limbs revealed shortening of the elements and unsegmented phalangeal elements (supplementary material Fig.S2D′, red arrows mark the unsegmented joints) compared to uninfected contralateral control (supplementary material Fig. S2B and B′, black arrow marks a segmented joint).

For molecular analysis, the region and extent of infection were assessed by immunohistochemistry against one of the viral gag proteins using 3C2 antibody (Fig. 1A). In the uninfected contralateral control joints the chick interzone is visualized as a, *COL2A1* negative, three layered structure comprising of a central intermediate layer (IL) flanked by

two OCL (Fig. 1B,B′, marked with dotted lines). The presence of such an organized three layered interzone could not be visualized in cNFIA-RNAi infected joints (Fig. 1E,E′). Moreover, knockdown of NFIA resulted in reduction in the *COL2A1* negative interzone (Compare the red line in Fig. 1B with Fig. 1E).

Furthermore, analysis of layer specific markers using RNA *in situ* hybridization exhibited loss of both the outer and intermediate layers of the interzone, following knockdown of NFIA, as demonstrated by downregulation of *PHLDA2*, an IL marker and *Finished cDNA clone ChEST302p20*, an OCL marker (Compare Fig. 1C,C′ with Fig. 1F,F′ and Fig. 1D,D′ with Fig. 1G,G′ respectively). In extreme cases, complete loss of *COL2A1* negative domain across some of the tibia-tarsus infected joint was observed (supplementary material Fig. S3A,A′).

While analyzing the expression of *COL2A1* transcripts in cNFIA-RNAi infected elements we noticed that the downregulation of *COL2A1* expression at the center of the elements (the arrows in Fig. 2A), which is typically associated with onset of hypertrophic differentiation, did not take place (compare Fig. 2A,A′). Thus, we investigated the status of hypertrophic differentiation in cNFIA-RNAi infected elements. RNA *in situ* hybridization of *IHH* revealed that the expression was not downregulated at the center of the element, the putative hypertrophic region (compare Fig. 2B,B′; yellow and red arrowheads). ColX immunoreactivity could not be detected in cNFIA-RNAi infected elements (compare Fig. 2D,D′; yellow and red arrowheads). Since Pthrp-PthrpR signaling plays a critical role in hypertrophic differentiation (Kronenberg, 2003), we investigated the mRNA expression of Pthrp and PthrpR. We could not detect any variation in Pthrp expression (data now shown) but expression of PthrpR was clearly downregulated in cNFIA-RNAi infected elements (compare Fig. 2C,C′; yellow and red arrowheads).

Nfia gain-of-function promotes chondrogenesis

Next, to assess whether NFIA gain-of-function can promote ectopic or expanded articular cartilage domain, HH14 chick limb buds were infected with RCAS retroviral particles expressing mouse-*Nfia* cDNA (m*Nfia*). The embryos were harvested at HH36. Misexpression of RCAS-m*Nfia* resulted in micromelia of the infected limbs (compare supplementary material Fig. S2E,G) and skeletal prep analysis of these infected limbs revealed a decrease in the alizarin red staining (marked by a red asterisk, supplementary material Fig. S2H′), along with shortened unsegmented skeletal elements (supplementary material Fig. S2H,H′, marked by arrows in 2H′) compared to uninfected contralateral control limb (supplementary material Fig. S2F,F′).

To assess molecular changes caused by *mNfia* misexpression we harvested RCAS-m*Nfia* infected as well as uninfected contralateral limbs (control). Region of infection within cartilage was assessed by (1) detecting expression of m*Nfia* transcripts (Fig. 3A′) and (2) detecting 3C2 immunoreactivity (Fig. 3H″, green). In agreement with observed unsegmented skeletal elements (supplementary material Fig. S2H´) we found that upon *mNfia* infection expression of several articular cartilage/ interzone specific markers such as *Gdf5*, *Bmp4* and *Sfrp2* were downregulated (compare Fig. 3B-D with Fig. 3B′-D′) in the putative joint region (marked by black arrows in Fig. 3B′-D′). Thus, contrary to our expectation, we could not detect ectopic expression of any of the articular cartilage markers in the infected cells.

It should also be noted that upon *mNfia* misexpression often the cells of the putative interzone region assumed a rounded morphology akin to cells in the epiphysis region (Fig. 3E′, marked by black arrow) as opposed to densely packed flattened morphology of interzone cells (Fig. 3E). These molecular and histological changes were particularly apparent in the phalangeal joints as opposed to more proximal joints. Moreover, these RCAS-m*Nfia* infected cells also expressed, an early transient cartilage marker, *COL2A1* (compare Fig. 3F,F′). The cell autonomous effect of *mNfia* misexpression is best exemplified in a joint that is partially infected. In such a joint the region that remained uninfected, the articular chondrocytes not only maintained their densely packed flattened morphology (Fig. 3E′, marked by red arrow) but also were *COL2A1* negative (Fig. 3F′, marked by red arrow) whereas the adjoining infected interzone cells (marked with black arrow in Fig. 3A′) adopted transient cartilage like morphology (Fig. 3E′, marked with black arrow) and expressed *COL2A1* (Fig. 3F′, marked with black arrow).

The interzone or developing articular cartilage is largely non-proliferative in contrast to adjacent transient cartilage cells (Ray et al., 2015). As misexpression of *mNfia* led to downregulation of several articular cartilage markers and ectopic expression of *COL2A1* we proceeded to determine the status of BMP signaling and cell proliferation in RCAS-*mNfia* infected putative interzone cells. For this purpose, we carried out immunohistochemistry for pSMAD1/5/8, a read-out of BMP signaling and phosphohistone H3 (pH3), a mitotic marker. As expected, we could detect ectopic pSMAD1/5/8 immuno-reactivity (compare Fig. 3G,G′ and G″) along with phosphohistone H3 (compare Fig. 3H,H′) in putative joint sites in *mNfia* infected tissues (marked by 3C2 immunostaining in green in Fig. 3H″).

Nfia gain-of-function blocks the differentiation of chondrocytes into prehypertrophic state and maintains the chondrocytes in a stable immature state

Skeletal analysis of m*Nfia* infected limbs revealed a decrease in alizarin red staining (supplementary material Fig. S2H,H´). Therefore, we investigated the molecular changes associated with endochondral ossification. Expression of *COL2A1* transcripts, which is normally reduced upon onset of hypertrophy, did not decrease from the epiphysis to the diaphysis of RCAS-m*Nfia* infected cartilage elements (compare Fig. 4A,A′).

In keeping, analysis of *IHH* and ColX expression revealed that misexpression of *mNfia* blocked prehypertrophic chondrocyte differentiation. We observed a marked decrease in the expression of *IHH* transcripts (Fig. 4B′) and *ColX* protein (Fig. 4C′) in the infected transient cartilage cells compared to uninfected contralateral cartilage element (compare Fig. 4B,B′ and Fig. 4C,C′). Thus, although RCAS-m*Nfia* infected cells continue to express *COL2A1* they do not progress further with transient cartilage differentiation program and were arrested in an initial chondrogenic state.

Several lines of investigation have demonstrated that both Ihh and Pthrp block hypertrophic differentiation of cartilage and that Ihh can induce expression of *PTHrP* in periarticular region through long range negative feedback loop (Lanske et al., 1996; Vortkamp et al., 1996; St-Jacques et al., 1999; Dentice et al., 2005; Koziel et al., 2005). Thus, we hypothesized that misexpression of *mNfia* might be affecting this Ihh/Pthrp regulatory loop. Hence, we next analyzed the expression pattern of Pthrp in *mNfia* misexpressed limbs. As expected, loss of *IHH* resulted in reduced expression of *PTHrP* in RCAS-m*Nfia* infected joints (compare Fig. 4D,D′, marked by black arrow).

Identification of *GATA3* as an articular cartilage specific gene and generation of *GATA3* gain-of-function and loss-of-function constructs

Bonilla-Claudio et al., recently reported *Gata3* to be a direct transcriptional target of BMP signaling during intramembranous ossification (Bonilla-Claudio et al., 2012). While investigating if *GATA3* is also expressed during endochondral ossification in a BMP signaling dependent manner, we discovered that *GATA3* is in fact expressed specifically in the developing articular cartilage/interzone of chick (Fig. 5A-E) and mouse (supplementary material Fig. S6A and A′). Further, *Gata3* has been suggested to promote the expression of 16 genes that are expressed in the articular cartilage (supplementary material table S1) in a previous microarray transcriptomic profiling of whole mammary glands (Kouros-Mehr et al., 2006). Thus, *GATA3* was an obvious candidate gene to be investigated for a possible role in inducing articular cartilage fate.

In order to study the effects of loss-of-function of GATA3 with respect to chicken embryonic articular cartilage development, we adopted a strategy for creating a dominant-negative version of GATA3 transcription factor as described by Kamei et al., 2011 (Kamei et al., 2011). Alignment of the amino-acid sequences of chick and mouse GATA3 DNA binding domains exhibits a sequence identity of 100%. Therefore, in order to generate a dominant-negative form of GATA3, we fused the DNA binding domain of mouse *Gata3* to the Engrailed transcriptional repressor domain (*mGata3*-EnR) (supplementary material Fig. S4C).

Gata3 loss-of-function results in the absence of joint and loss of articular cartilage markers

The existing data indicating that loss of *Gata3* expression is associated with downregulation of expression of 16 articular cartilage markers (Kouros-Mehr et al., 2006 and supplementary material table S1) suggested that Gata3 plays an instructive role in articular cartilage differentiation. To investigate whether GATA3 is necessary for chick articular cartilage development we misexpressed *mGata3*-EnR in the prospective limb field by electroporation of RCAS-mGata3-EnR construct at HH14. The efficiency of electroporation was assessed by co-electroporating a pCAGGS-mCherry reporter construct (supplementary material Fig. S1, also refer to Experimental Procedures). The embryos were harvested at HH36. Electroporation of embryonic limb buds with RCAS-*mGata3*-EnR construct consistently resulted in digit truncation and interdigital syndactyly (supplementary material Fig. S5C). In extreme cases we also observed hemangioma/blood pooling at the distal end of an infected limb (supplementary material Fig. S5B). Whole mount skeletons of RCAS-*Gata3*-EnR electroporated limbs stained with alcian blue and alizarin red revealed a decrease in alizarin red staining (supplementary material Fig. S5B′, marked by red asterisks) along with unsegmented skeletal elements (supplementary material Fig. S5C′, marked by black arrows) compared to the uninfected contralateral control (supplementary material Fig. S5A,A′).

To analyze molecular and histological changes brought about by GATA3 loss-of-function we analyzed sections of *mGata3*-EnR infected limbs. Region of infection within cartilage was assessed by both detecting expression of *mGata3* mRNA (Fig. 5J′) and by 3C2 immunoreactivity (Fig. 5L″,L‴). Expression of dominant negative GATA3, *mGata3*-EnR, resulted in ectopic expression of transient cartilage marker *COL2A1* (compare Fig. 5F,F′),

and the absence of joint specific markers *SFRP2*, *ENPP2*, *GDF5* (compare Fig. 5G-I and Fig. 5G′-I′) in the putative joint region cells (marked by black arrows).

Moreover, we observed that *Gata3*-EnR infected interzone cells are mitotically active, as assessed by pH3 immunoreactivity (Fig. 5L,L′), and are pSMAD1/5/8 positive (Fig. 5K,K′), thus mimicking the attributes of transient cartilage. It should be noted that in *mGata3*-EnR limbs normal hypertrophic differentiation was unaffected (data not shown).

Gata3 gain-of-function results in the appearance of ectopic articular cartilage markers

Having established that GATA3 loss-of-function results in downregulation of several articular cartilage markers, next we asked whether misexpression of *GATA3* can promote ectopic or expanded domain of articular cartilage markers. For this purpose, we misexpressed *mGata3* cDNA in HH14 limb buds (RCAS-*mGata3*) and harvested the embryos at HH36. Misexpression of *mGata3* in limb buds did not result in particularly striking overt phenotype apparent in the whole mount (data not shown). Thus, we used pCAG-mCherry as an electroporation marker and analyzed limb buds that were well electroporated. We generated sections from such limbs and analyzed for molecular changes. Region of infection within sections of limb cartilage was assessed by *mGata3* RNA *in situ* hybridization (Fig. 6A′). Analysis of articular cartilage specific markers revealed mild ectopic expression of *c-JUN* and *WNT9A* mRNAs within the domains of *mGata3* misexpression (Compare Fig. 6B-C and Fig. 6B′-C′). Further, we also observed weak ectopic β-catenin immunoreactivity in the cells surrounding the ectopic domains of *c-JUN* and *WNT9A* expression (Compare Fig. 6D and Fig. 6D′). However, it should be noted that while misexpression of *mGata3* resulted in ectopic expression of *c-Jun* and *Wnt9a*, it did not stimulate ectopic expression of many other articular cartilage markers (supplementary material Fig. S6B-F).

We thus speculated that GATA3 alone may not be sufficient to promote articular cartilage differentiation and needs other transcriptional collaborators. To investigate this possibility we fused the DNA binding domain of *mGata3* to the VP16 transcriptional activator domain (*mGata3*-VP16) (supplementary material Fig. S4B) (Kamei et al., 2011). Such fusion proteins are directed to their cognate DNA binding sites, in an enhancer, due to the presence of the DNA binding domain wherein they activate transcription from such enhancers irrespective of the presence of other collaborating transcription factors and thus act as constitutively active version of the transcription factor.

We introduced RCAS-*mGata3*-VP16 construct in the HH14 limb buds and harvested the embryos at HH36. Inspection of freshly harvested unfixed, unstained RCAS-*mGata3*-VP16 infected limbs revealed micromelia (shortened limb elements), interdigital syndactyly and hematoma/hemorrhage in the infected limb (supplementary material Fig. S5E) as compared to the uninfected contralateral control limb (supplementary material Fig. S5D). Whole mount skeletons of RCAS-*mGata3*-VP16 infected limbs stained with alcian blue and alizarin red revealed a decrease in alizarin red staining along with shortened unsegmented skeletal elements (supplementary material Fig. S5E′) compared to the uninfected contralateral control (supplementary material Fig. S5D′).

Region of infection within sections of limb cartilage was assessed by 3C2 immunoreactivity (Fig. 7A″-C″). We observed misexpression of constitutively active *mGata3* resulted in the ectopic expression of four joint specific markers, namely *SFRP2, c-JUN, CCNI* and *ENPP2* (marked within a dotted box, compare Fig. 6F-I and Fig. 6F′-I′). It should be noted that despite rather broad domains of misexpression of *mGata3*-VP16, ectopic expression of the joint specific markers was found to be present only near the putative joint site. On the other

hand expression of some of the other articular cartilage markers such as *PTHrP*, *NFIA*, *PHLDA2* and *Finished cDNA clone ChEST302p20* remained unaltered (compare Fig. 6J-K and Fig. 6J′-K′, and data not shown). Moreover, this ectopic expression of articular cartilage markers was accompanied with a slight downregulation of *COL2A1*, a transient cartilage marker, in the m*Gata3*-VP16 infected cells near the future joint region (compare Fig. 6E,E′).

As stated before, from previous analyses, we already knew that in contrast to transient cartilage, articular cartilage cells are largely non-proliferative, β-catenin positive and pSMAD1/5/8 negative (Ray et al., 2015). Thus, we wanted to assess whether *mGata3*-VP16 infected putative transient cartilage cells, which expressed ectopic articular cartilage markers also attained these attributes of articular cartilage. In order to assess proliferation, we labeled the dividing cells in the embryo with EdU, a thymidine analogue. Akin to articular cartilage cells in the contralateral limb (region marked by white arrows between dotted lines, Fig. 7C) the number of EdU positive cells were found to be downregulated in *mGata3*-VP16 infected cells (Fig. 7C′,C″). Moreover, this downregulation of EdU in *mGata3*-VP16 infected cells was accompanied by ectopic induction of *WNT9A* (supplementary material Fig. S6G-J) and β-catenin (Fig. 7A,A′) along with downregulation of pSMAD1/5/8 (Fig. 7B,B′). Overall, these lines of evidence suggest that Gata3 gain-of-function promotes articular cartilage fate at the expense of transient cartilage.

Gata3 gain-of-function blocks chondrocyte differentiation from prehypertrophic to hypertrophic state

In an uninfected contralateral control cartilage anlagen *COL2A1* expression gradually decreases from the epiphysis towards the center of the cartilage element where hypertrophic differentiation takes place (Fig. 7D). We observed that misexpression of constitutively active *Gata3* blocks such downregulation of *COL2A1* expression (Fig. 7D′). Furthermore,

misexpression of *mGata3*-VP16 arrested the chondrocytes in prehypertrophic state marked by a contiguous band of *IHH* expressing cells, within the center of the cartilage element (Fig. 7E′, marked by red arrows) and blocked further transition to hypertrophic state as demonstrated by absence of ColX (Fig. 7F′, marked by red arrow) in contrast to control where *IHH* is expressed as two discrete bands (Fig. 7E, marked by yellow arrows) with ColX expressed in the center (Fig. 7F, marked by yellow arrow). These observations are somewhat similar to what was observed in NFIA loss-of-function limb skeletons (compare, Fig. 2A,B,D and Fig. 2A′,B′,D′). It should however be noted that though *mGata3*-VP16 was misexpressed even in the prehypertrophic region, the articular cartilage markers were not ectopically expressed in these domains.

DISCUSSION

Transcriptional regulation of articular cartilage differentiation and maintenance is not well understood. Earlier, we reported identification of *NFIA* as an articular cartilage specific transcription factor (Singh et al., 2016). In this report, we identified *GATA3* as another transcription factor that is specifically expressed in the chick and mouse articular cartilage and characterized the roles of NFIA and GATA3 during chick articular cartilage differentiation. Our data suggest that NFIA although not sufficient for articular cartilage differentiation but is necessary to maintain the permanent fate of articular cartilage through prevention of hypertrophic differentiation. On the other hand, gain-of-function and loss-of-function experiments demonstrated that GATA3 is necessary for articular cartilage differentiation and requires cooperation of other unknown activation factors to promote articular cartilage differentiation.

Role of NFIA in joint development

Knockdown of chick NFIA reduces or abrogates the *COL2A1* negative interzone domain while misexpression of NFIA prevents hypertrophic differentiation of the transient cartilage cells. Taken together, it appears that NFIA primarily aids in maintenance of articular cartilage fate by preventing hypertrophic differentiation of interzone/articular cartilage cells.

Nfia is expressed specifically in 16.5 dpc mouse articular cartilage as well (supplementary material Fig. S3C,C′). However, unlike knockdown of NFIA in chick embryos, disruption of NFIA gene in mice did not result in dramatic phenotype but it appears that in the absence of Nfia mild disruption of the organization of articular cartilage occurs (supplementary material Fig. S3E-H and S3E′-H′). This rather mild morphological defect in skeletal and cartilage elements may be due to redundancy (das Neves et al., 1999). It should be noted that Nfia has several homologues e.g. Nfib, Nfic and Nfix. We have also detected expression of *Nfix* in mouse articular cartilage (supplementary material Fig. S3D,D′). It will be interesting to analyze the effects of compound knockouts of combinations of these factors in articular cartilage differentiation.

Misexpression of *mNfia* in developing chick limb skeleton promoted ectopic expression of *COL2A1* transcripts in the putative interzone/articular cartilage cells. This is paradoxical considering embryonic articular cartilage does not express *Col2a1* mRNA. It should be noted that while some of the articular cartilage specific genes such as Wnt9a, Wnt4 and Wnt16 are anti-chondrogenic in nature, there are others like Gdf5 and Gdf6 which are chondrogenic. Ectopic chondrogenesis and abrogation of articular joint formation upon overexpression of NFIA is very similar to what is observed with GDF5 overexpression (Francis-West et al., 1999; Merino et al., 1999; Storm and Kingsley, 1999; Tsumaki et al., 1999). However, Gdf5

misexpression is not reported to cause block in hypertrophy. C-1-1 was proposed to be a Gdf5 target and its misexpression causes block in hypertrophy similar to what we observed in NFIA misexpression but the effect of C-1-1 misexpression on ectopic chondrogenesis (ectopic *Col2a1* expression) has not been reported (Iwamoto et al., 2001; Iwamoto et al., 2000). Finally, just like NFIA, both gain- and loss-of-function manipulations of GDF5 cause abrogation of joint formation. The broad similarity in the articular cartilage developmental defects upon gain- or loss-of-function manipulations of GDF5, ERG or NFIA raises the question whether these genes functionally interact for proper articular cartilage development (Fig. 8).

Role of GATA3 in joint development

Germline deletion of *Gata3* in mice results in embryonic lethality by the time joint development initiates in the limbs precluding analysis of its role in articular cartilage differentiation (Pandolfi et al., 1995). A limb-specific knockout of *Gata3* needs to be generated. In the absence of such a mouse model we decided to take advantage of the chick embryonic system. We made several attempts to knockdown GATA3 by miRNA, similar to what we did for NFIA, but without any success. We thus generated *mGata3*-EnR construct which serves as a dominant negative form of GATA3 by repressing transcription of Gata3 downstream genes. Such a strategy has earlier been used for Gata4 (Kamei et al., 2011). Infection with *mGata3*-EnR in chicken limbs resulted in spectrum of malformations, where some of the characteristics were similar to Gata3 knockout mice, such as pooling of blood, hemorrhages and smaller size of the elements (Pandolfi et al., 1995). It is interesting that both Gata3 gain- and loss-of-function resulted in inhibition of certain joint formation. In this context, it should be noted that in 1993, Macias et. al., reported that application of Retinoic Acid (RA) in the interdigital mesenchyme resulted in inhibition of joint formation. It is

known that many of the Gata factors, including Gata4/6, are transcribed in RA dependent manner (Arceci et al., 1993; Mauney et al., 2010) . Thus, it would be interesting to investigate if RA can induce Gata3 in early limb skeletal anlagen and if that affects joint induction. In contrast, we speculate that Gata3 loss-of-function induces ectopic BMP signaling domain, thus eliminating a permissive environment for joint induction (Ray et al., 2015).

In the 50 kb genomic region upstream of the mouse and human Gata3 genes five conserved regions containing 10 putative TCF/Lef binding sites were identified using bioinformatics analysis (Grote et al., 2008). Therefore, Gata3 transcription is speculated to be regulated by Wnt signaling through β-catenin. Misexpression of *Wnt9a* or β-catenin in the limb results in ectopic expression of articular cartilage markers such as *Autotaxin* (*Enpp2*) and *Sfrp2* (Hartmann and Tabin, 2001). Interestingly, we observed that misexpression of *mGata3* promotes ectopic expression of *c-JUN*, *WNT9A* and β-catenin. This suggests that *GATA3* is not only downstream of Wnt/β-catenin signaling, but also maintains it in a feedback loop via c-*JUN*. Further, since *c-Jun* is known to promote expression of Wnt ligands (Kan and Tabin, 2013) thus ectopic expression of *Wnt9a* and β-catenin may be an indirect effect of c-Jun activation by Gata3. Moreover, we observed that while *mGata3* could induce ectopic expression of a few articular cartilage specific genes, more articular cartilage specific genes were ectopically expressed when a constitutively active version of *mGata3* was misexpressed (*mGata3*-VP16). Since VP16 fusion allows a transcription factor to activate transcription even in the absence of other collaborating transcription factors we speculate that GATA3, in addition to activating expression of *c-JUN*, acts in conjunction with other transcription factors to promote articular cartilage differentiation. We have routinely observed that GATA3 gain-of-function induces ectopic expression of articular cartilage specific genes only in the vicinity of the interzone and not in cells away from it. This suggests that only these cells are competent, while the cells away from the joint site are not competent, to upregulate

expression of articular cartilage specific genes even upon misexpression of constitutively activated form of *Gata3* further underscoring the importance of context and/or presence of other transcription factors.

As of now three transcription factors expressed in the joint interzone have been identified, namely C-1-1 variant of *ERG*, *OSR1/2* and *c-JUN*, to play important roles during articular cartilage differentiation (Iwamoto et al., 2000; Iwamoto et al., 2001; Iwamoto et al., 2007; Gao et al., 2011; Kan and Tabin, 2013). C-1-1 misexpression prevents hypertrophic differentiation but does not promote ectopic expression of articular cartilage specific genes other than Tenascin-C (Iwamoto et al., 2000; Iwamoto et al., 2007). However, articular cartilage specific ablation of ERG does not affect the embryonic articular cartilage differentiation but leads to OA like phenotypic defects in 11 month mice (Ohta et al., 2015). On the other hand c-JUN, presumably due to its ability to promote transcription of Wnt ligands, Wnt9a and Wnt16, is necessary for articular cartilage differentiation (Kan and Tabin, 2013). However, as no gain-of-function study has been conducted it is unclear if c-JUN is sufficient for articular cartilage differentiation. c-JUN loss-of-function spares specification of interzone. *OSR1/2* compound knockout abrogates joint formation and promotes ectopic transient cartilage differentiation in the putative joint region (Gao et al., 2011). Nonetheless, since OSR1/2 loss-of-function reduces expression of Wnt ligands and since β-catenin loss-of-function did not affect OSR1/2 expression it is likely that OSR1/2 acts upstream of Wnt ligand expression and collaborates with transcriptional targets of Wnt signaling pathway to promote articular cartilage differentiation (Gao et al., 2011). Since OSR1/2 misexpression studies have not been carried out it is difficult to assess whether OSR1/2 can induce articular cartilage fate like GATA3. By conducting both loss- and gain-of-function analyses we have demonstrated that NFIA and GATA3 act at two different levels during articular cartilage differentiation. NFIA, similar to C-1-1, acts by preventing hypertrophic differentiation in

articular region while GATA3 promotes articular cartilage fate by activating expression of several articular cartilage specific genes. However, GATA3 needs to collaborate with other transcription factors for these. It remains to be seen whether OSR1/2 and c-JUN are such transcription factors (Fig. 8).

Crosstalk between articular cartilage and transient cartilage differentiation

Gain- or loss-of-function of NFIA and gain-of-function of GATA3 not only affected articular cartilage differentiation but also affected hypertrophic differentiation, albeit at different levels. The role of Ihh/Pthrp feedback loop in controlling hypertrophic differentiation is well established (Kronenberg, 2003). However, it is unlikely that these are the only two players to be involved in the process. Ihh loss-of-function causes absence of articular joint (St-Jacques et al., 1999; Koyama et al., 2007). This is unlikely due to the effect of Ihh on Pthrp expression as Pthrp is not known to promote articular cartilage differentiation. Rather it is likely that loss-of-function of Ihh is affecting some factor(s) which is directly or indirectly responsible for articular cartilage differentiation. Unfortunately, we could not find any data in the literature that describes changes in Ihh expression upon gain or loss of ERG function but interestingly loss of Ihh does not cause loss of ERG C-1-1 expression (Koyama et al., 2007). In keeping, gain-of-function of C-1-1, ERG variant, blocks hypertrophic differentiation but does not affect articular cartilage differentiation while NFIA gain-of-function not only blocks hypertrophic differentiation but also affects articular cartilage differentiation. In the context of medulla blastoma, *Ptch1* is reported to regulate *Nfia* expression (Genovesi et al., 2013). Thus, it is possible that NFIA is one of the regulators of the crosstalk between articular cartilage and hypertrophic cartilage differentiation. In this context it is interesting to note that loss of GATA3 function did not affect hypertrophy while loss of NFIA did. As NFIA and GATA3 seem to act at different stages of articular cartilage differentiation it is possible that GATA3 loss-of-function, though blocks articular cartilage differentiation but does not affect

expression of the factors that control hypertrophic differentiation e.g. PTHrP or IHH. It is worth noting that GATA3 gain-of-function did not affect NFIA expression (Fig. 6). Gain-of-function of GATA3 causes ectopic articular cartilage differentiation as well as block in hypertrophy. However, our data cannot rule out the possibility that these are two unconnected events. Unfortunately, we could not obtain any embryo where *mGata3*-VP16 is misexpressed only in the hypertrophic cartilage and not in the articular cartilage.

In summary, it appears that a network involving GATA3, OSR1/2, c-JUN, WNT ligands regulates articular cartilage differentiation, another network involving NFIA, GDF5, ERG prevent transient cartilage differentiation in articular cartilage domain and a third network involving IHH, PTHrP, NFIA and C-1-1 controls the cross-talk between articular cartilage differentiation and hypertrophy. The network that controls articular cartilage differentiation is becoming clearer. However, the mechanism of action of the network that prevent ectopic hypertrophy in the articular cartilage domain and the one that controls the cross-talk between articular cartilage and hypertrophic cells remain enigmatic. Our study provides possible new avenues for investigation into these aspects.

EXPERIMENTAL PROCEDURES

Tissues

Fertilized White Leghorn Chicken eggs were obtained from Central Avian Research Institute of India; Chandra Shekhar Azad Agricultural University, Kanpur, UP and Ganesh Enterprises, Nankari, Kanpur, UP. Eggs were incubated at 38°C in a humified chamber to be treated and/or harvested at specific stages of development assessed by Hamburger and Hamilton staging criteria (Hamburger and Hamilton, 1951).

Mouse experiments were conducted as per protocol approved by the Institute Animal Ethics Committee (registration number CPCSEA-56/1999). $Nfia^{-/+}$ male and female mice were mated, embryos were harvested at 16.5 dpc and genotyped (das Neves et al., 1999) to identify $Nfia^{-/-}$ and wild-type ($Nfia^{+/+}$).

Alcian Blue and Alizarin Red staining

The embryos were harvested and eviscerated in PBS and fixed in 95% ethanol for at least 2-3 days followed by an overnight fixation in 100% acetone. Next, the tissues were stained for 2-3 days within a mixture of 1 volume of 0.3% alcian blue 8GX (Sigma-Aldrich) solution in 95% ethanol: 1 volume of 0.1% alizarin red solution in 70% ethanol: 1 volume of glacial acetic acid: 17 volumes of 70% ethanol. Post-staining the tissues were cleared in 1% potassium hydroxide and photographed under a dissection microscope.

Tissue processing

Embryonic limbs were dissected and fixed overnight in 4% paraformaldehyde at 4˚C, embedded in paraffin and 5-10 µm sections cut along the para-sagittal plane using a microtome.

RNA *in situ* hybridization

cDNA clones used to make digoxigenin labelled antisense riboprobes generated by *in vitro* transcription are detailed in Table S2. RNA *in situ* hybridization was performed as described previously (Singh et al., 2016). RNA *in situ* hybridization signal for a given probe on the control and the test sections were developed on the same slide.

Immunohistochemistry

For pSMAD1/5/8, β-catenin, Noggin and GFP immunohistochemistry, sections were processed and detected as described in (Ray et al., 2015).

Immunohistochemistry

Sections were deparaffinized and were rehydrated in PBS, followed by post-fixation in 4% PFA. Sections were incubated overnight at 4°C with the following primary antibodies: anti-pH3 (Sigma-Aldrich, H0412; 1:100), anti-β-catenin-Cy3 (Sigma Aldrich, C7738; 1:200), anti-GAG (3C2; Potts et al., 1987), anti-pSMAD1/5/8 (Cell Signaling, 9511; 1:100) and anti-ColX (DSHB Hybridoma Product X-AC9 deposited by Linsenmayer, T.F; 1:20). Following this step, tissues were washed in PBT and incubated with respective secondary antibodies, such as DyLight 549 AffiniPure goat anti-rabbit IgG (Jackson ImmunoResearch Laboratories, 111-505-003; 1:200 for anti-pSMAD158 and anti-pH3; Alexa Fluor® 488 conjugated anti-mouse IgG (Jackson Immunoresearch Laboratories, Cat. no. 115-545-003) for 3C2 and DyLight549 conjugated anti-mouse IgG (Jackson Immunoresearch Laboratories,

Cat. no. 115-505-003) for anti-ColX. The tissues were counterstained with DAPI and mounted in VECTASHILED antifade reagent (Vector Laboratories, USA: H-1000).

EdU labelling

EdU (E10415, C10083, Invitrogen) labelling and detection was performed as previously described (Ray et al., 2015).

Viral misexpression

DF1 (Himly et al., 1998), chicken embryo fibroblast cells were checked to ensure they are free of contamination. Cells were transfected with RCAS-HA-m*Nfia* construct obtained from Benjamin Deneen (Deneen et al., 2006). Virus particles were produced, concentrated and titered as described previously (Logan and Tabin, 1998). The embryos were lowered by removing 2-3 ml of albumin and a window was made through which viral solutions having a titer of 1 X 10^8 IU/ml mixed with 1% fast green was injected into the lateral Plate Mesoderm (LPM) of HH10 embryos which is destined to give rise to the prospective hindlimb of the embryo.

In ovo electroporation

The embryos were initially lowered by removing 2-3 ml of albumin and a window was made to visualize the embryo under the vitelline membrane. This vitelline membrane was shorn near the hindlimb field and bathed in 100µl sterile PBS + Pen Strep solution (Thermo Fisher Scienific, Cat. no: 10378016). At stage HH14 RCAS constructs RCAS-HA-m*Nfia* or RCAS-*NFIA* shRNAi (target region within NFIA CDS- GCCATCGCCAACTGCATTAAA) obtained from Benjamin Deneen (Deneen et al., 2006) or RCAS-GATA3-DBD-VP16 or RCAS-GATA3-DBD-EnR mixed with 0.5µg/µl pCAGGS-mCherry and 0.1% fast green was injected into the embryonic space between the somatic LPM and splanchnic LPM at a concentration of 2µg/µl using a microinjector. Electroporation was performed as described (Suzuki and Ogura, 2008).

ACKNOWLEDGMENTS

We are grateful to Prof. Andrew Lassar, Harvard Medical School, USA for sharing full length mouse GATA3 construct and to Prof. Benjamin Deneen, Baylor College of Medicine, Houston, TX, US, for providing the RCAS-mNFIA and RCAS-cNFIAshRNAi constructs. We thank Prof. Richard Gronostajski for permission to obtain *Nfia* mutant mice from Prof.

Shubha Tole. Work was supported by grants from the Department of Biotechnology, India (DBT) BT/PR11202/MED/32/46/2008 and from Science and Engineering Research Board of Department Science and Technology of Govt. of India (EMR/2015/001519 to A.B.). P.N.P.S. was supported by fellowship from Council of Scientific & Industrial Research (CSIR), India. U.S.Y. and K.A. were supported by fellowship from the Ministry of Human Resource Development (MHRD), India and VK was supported by University Grants Commission (UGC) fellowship, India.

AUTHOR CONTRIBUTIONS

P.N.P.S. and A.B. designed the experiments. P.N.P.S., U.S.Y, K.A. and P.G. performed the chick experiments. P.N.P.S. and V.K. performed the mouse experiments. P.N.P.S., U.S.Y. and A.B. interpreted data. P.N.P.S. and A.B. wrote the manuscript. P.N.P.S., U.S.Y. and A.B. reviewed and edited the manuscript.

REFERENCES

Arceci, R. J., King, A., Simon, M. C., Orkin, S. H. and Wilson, D. B. (1993) 'Mouse GATA-4: a retinoic acid-inducible GATA-binding transcription factor expressed in endodermally derived tissues and heart', *Mol Cell Biol* 13(4): 2235-2246.

Archer, C. W., Dowthwaite, G. P. and Francis-West, P. (2003) 'Development of synovial joints', *Birth Defects Res C Embryo Today* 69(2): 144-55.

Bi, W., Deng, J. M., Zhang, Z., Behringer, R. R. and de Crombrugghe, B. (1999) 'Sox9 is required for cartilage formation', *Nat Genet* 22(1): 85-9.

das Neves, L., Duchala, C. S., Tolentino-Silva, F., Haxhiu, M. A., Colmenares, C., Macklin, W. B., Campbell, C. E., Butz, K. G. and Gronostajski, R. M. (1999) 'Disruption of the murine nuclear factor I-A gene (Nfia) results in perinatal lethality, hydrocephalus, and agenesis of the corpus callosum', *Proceedings of the National Academy of Sciences of the United States of America* 96(21): 11946-51.

Deneen, B., Ho, R., Lukaszewicz, A., Hochstim, C. J., Gronostajski, R. M. and Anderson, D. J. (2006) 'The transcription factor NFIA controls the onset of gliogenesis in the developing spinal cord', *Neuron* 52(6): 953-68.

Dentice, M., Bandyopadhyay, A., Gereben, B., Callebaut, I., Christoffolete, M. A., Kim, B. W., Nissim, S., Mornon, J. P., Zavacki, A. M., Zeold, A. et al. (2005) 'The Hedgehog-inducible ubiquitin ligase subunit WSB-1 modulates thyroid hormone activation and PTHrP secretion in the developing growth plate', *Nat Cell Biol* 7(7): 698-705.

Francis-West, P. H., Abdelfattah, A., Chen, P., Allen, C., Parish, J., Ladher, R., Allen, S., MacPherson, S., Luyten, F. P. and Archer, C. W. (1999) 'Mechanisms of GDF-5 action during skeletal development', *Development* 126(6): 1305-15.

Gao, Y., Lan, Y., Liu, H. and Jiang, R. (2011) 'The zinc finger transcription factors Osr1 and Osr2 control synovial joint formation', *Dev Biol* 352(1): 83-91.

Genovesi, L. A., Ng, C. G., Davis, M. J., Remke, M., Taylor, M. D., Adams, D. J., Rust, A. G., Ward, J. M., Ban, K. H., Jenkins, N. A. et al. (2013) 'Sleeping Beauty mutagenesis in a mouse medulloblastoma model defines networks that discriminate between human molecular subgroups', *Proceedings of the National Academy of Sciences of the United States of America* 110(46): E4325-34.

Grote, D., Boualia, S. K., Souabni, A., Merkel, C., Chi, X., Costantini, F., Carroll, T. and Bouchard, M. (2008) 'Gata3 acts downstream of beta-catenin signaling to prevent ectopic metanephric kidney induction', *PLoS Genet* 4(12): e1000316.

Guo, X., Day, T. F., Jiang, X., Garrett-Beal, L., Topol, L. and Yang, Y. (2004) 'Wnt/beta-catenin signaling is sufficient and necessary for synovial joint formation', *Genes Dev* 18(19): 2404-17.

Hamburger, V. and Hamilton, H. L. (1951) 'A series of normal stages in the development of the chick embryo', *Journal of Morphology* 88(1): 49-92.

Hartmann, C. and Tabin, C. J. (2001) 'Wnt-14 plays a pivotal role in inducing synovial joint formation in the developing appendicular skeleton', *Cell* 104(3): 341-51.

Himly, M., Foster, D. N., Bottoli, I., Iacovoni, J. S. and Vogt, P. K. (1998) 'The DF-1 chicken fibroblast cell line: transformation induced by diverse oncogenes and cell death resulting from infection by avian leukosis viruses', *Virology* 248(2): 295-304.

Holder, N. (1977) 'An experimental investigation into the early development of the chick elbow joint', *Journal of Embryology and Experimental Morphology* 39: 115-27.

Iwamoto, M., Higuchi, Y., Enomoto-Iwamoto, M., Kurisu, K., Koyama, E., Yeh, H., Rosenbloom, J. and Pacifici, M. (2001) 'The role of ERG (ets related gene) in cartilage development', *Osteoarthritis Cartilage* 9 Suppl A: S41-7.

Iwamoto, M., Higuchi, Y., Koyama, E., Enomoto-Iwamoto, M., Kurisu, K., Yeh, H., Abrams, W. R., Rosenbloom, J. and Pacifici, M. (2000) 'Transcription factor ERG variants and functional diversification of chondrocytes during limb long bone development', *J Cell Biol* 150(1): 27-40.

Iwamoto, M., Tamamura, Y., Koyama, E., Komori, T., Takeshita, N., Williams, J. A., Nakamura, T., Enomoto-Iwamoto, M. and Pacifici, M. (2007) 'Transcription factor ERG and joint and articular cartilage formation during mouse limb and spine skeletogenesis', *Dev Biol* 305(1): 40-51.
Kamei, C. N., Kempf, H., Yelin, R., Daoud, G., James, R. G., Lassar, A. B., Tabin, C. J. and Schultheiss, T. M. (2011) 'Promotion of avian endothelial cell differentiation by GATA transcription factors', *Dev Biol* 353(1): 29-37.
Kan, A. and Tabin, C. J. (2013) 'c-Jun is required for the specification of joint cell fates', *Genes Dev* 27(5): 514-24.
Karsenty, G. and Wagner, E. F. (2002) 'Reaching a genetic and molecular understanding of skeletal development', *Dev Cell* 2(4): 389-406.
Kouros-Mehr, H., Slorach, E. M., Sternlicht, M. D. and Werb, Z. (2006) 'GATA-3 maintains the differentiation of the luminal cell fate in the mammary gland', *Cell* 127(5): 1041-55.
Koyama, E., Ochiai, T., Rountree, R. B., Kingsley, D. M., Enomoto-Iwamoto, M., Iwamoto, M. and Pacifici, M. (2007) 'Synovial joint formation during mouse limb skeletogenesis: roles of Indian hedgehog signaling', *Ann N Y Acad Sci* 1116: 100-12.
Koziel, L., Wuelling, M., Schneider, S. and Vortkamp, A. (2005) 'Gli3 acts as a repressor downstream of Ihh in regulating two distinct steps of chondrocyte differentiation', *Development* 132(23): 5249-60.
Kronenberg, H. M. (2003) 'Developmental regulation of the growth plate', *Nature* 423(6937): 332-6.
Lanske, B., Karaplis, A. C., Lee, K., Luz, A., Vortkamp, A., Pirro, A., Karperien, M., Defize, L. H., Ho, C., Mulligan, R. C. et al. (1996) 'PTH/PTHrP receptor in early development and Indian hedgehog-regulated bone growth', *Science* 273(5275): 663-6.
Mauney, J. R., Ramachandran, A., Richard, N. Y., Daley, G. Q., Adam, R. M. and Estrada, C. R. (2010) 'All-trans retinoic acid directs urothelial specification of murine embryonic stem cells via GATA4/6 signaling mechanisms', *PloS one* 5(7): e11513.
Merino, R., Macias, D., Ganan, Y., Economides, A. N., Wang, X., Wu, Q., Stahl, N., Sampath, K. T., Varona, P. and Hurle, J. M. (1999) 'Expression and function of Gdf-5 during digit skeletogenesis in the embryonic chick leg bud', *Dev Biol* 206(1): 33-45.
Ohta, Y., Okabe, T., Larmour, C., Di Rocco, A., Maijenburg, M. W., Phillips, A., Speck, N. A., Wakitani, S., Nakamura, T., Yamada, Y. et al. (2015) 'Articular cartilage endurance and resistance to osteoarthritic changes require transcription factor Erg', *Arthritis Rheumatol* 67(10): 2679-90.
Pacifici, M., Koyama, E. and Iwamoto, M. (2005) 'Mechanisms of synovial joint and articular cartilage formation: recent advances, but many lingering mysteries', *Birth Defects Res C Embryo Today* 75(3): 237-48.
Pandolfi, P. P., Roth, M. E., Karis, A., Leonard, M. W., Dzierzak, E., Grosveld, F. G., Engel, J. D. and Lindenbaum, M. H. (1995) 'Targeted disruption of the GATA3 gene causes severe abnormalities in the nervous system and in fetal liver haematopoiesis', *Nat Genet* 11(1): 40-44.
Pitsillides, A. A. and Beier, F. (2011) 'Cartilage biology in osteoarthritis--lessons from developmental biology', *Nat Rev Rheumatol* 7(11): 654-63.
Ray, A., Singh, P. N., Sohaskey, M. L., Harland, R. M. and Bandyopadhyay, A. (2015) 'Precise spatial restriction of BMP signaling is essential for articular cartilage differentiation', *Development* 142(6): 1169-79.
Shubin, N. H., and Alberch, P. (1986) 'A morphogenetic approach to the origin and basic organization of the tetrapod limb.', *Evolutionary Biology* 20: 319-387.
Singh, P. N., Ray, A., Azad, K. and Bandyopadhyay, A. (2016) 'A comprehensive mRNA expression analysis of developing chicken articular cartilage', *Gene Expr Patterns* 20(1): 22-31.
Spater, D., Hill, T. P., Gruber, M. and Hartmann, C. (2006a) 'Role of canonical Wnt-signalling in joint formation', *Eur Cell Mater* 12: 71-80.
Spater, D., Hill, T. P., O'Sullivan R, J., Gruber, M., Conner, D. A. and Hartmann, C. (2006b) 'Wnt9a signaling is required for joint integrity and regulation of Ihh during chondrogenesis', *Development* 133(15): 3039-49.

St-Jacques, B., Hammerschmidt, M. and McMahon, A. P. (1999) 'Indian hedgehog signaling regulates proliferation and differentiation of chondrocytes and is essential for bone formation', *Genes Dev* 13(16): 2072-86.
Storm, E. E. and Kingsley, D. M. (1999) 'GDF5 coordinates bone and joint formation during digit development', *Dev Biol* 209(1): 11-27.
Suzuki, T. and Ogura, T. (2008) 'Congenic method in the chick limb buds by electroporation', *Development Growth & Differentiation* 50(6): 459-65.
Tsumaki, N., Tanaka, K., Arikawa-Hirasawa, E., Nakase, T., Kimura, T., Thomas, J. T., Ochi, T., Luyten, F. P. and Yamada, Y. (1999) 'Role of CDMP-1 in skeletal morphogenesis: promotion of mesenchymal cell recruitment and chondrocyte differentiation', *J Cell Biol* 144(1): 161-73.
Vortkamp, A., Lee, K., Lanske, B., Segre, G. V., Kronenberg, H. M. and Tabin, C. J. (1996) 'Regulation of rate of cartilage differentiation by Indian hedgehog and PTH-related protein', *Science* 273(5275): 613-22.

Figures

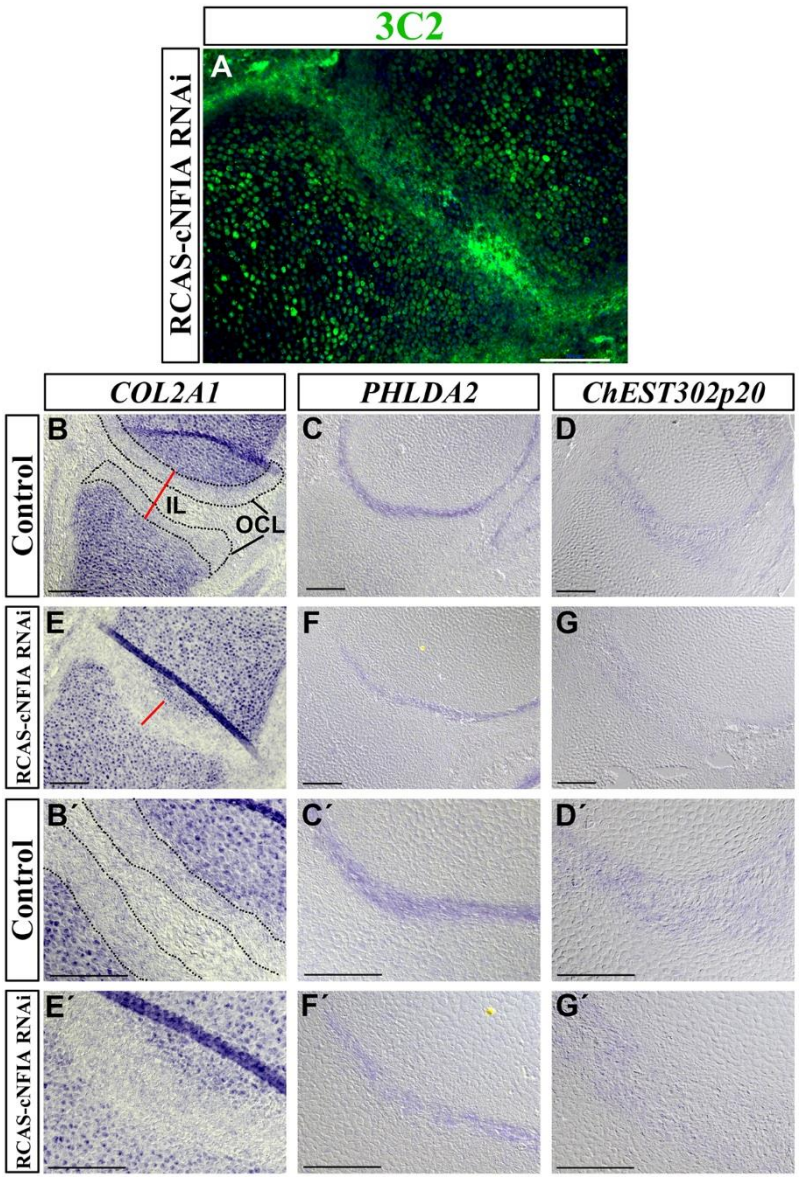

Fig. 1. NFIA loss-of-function leads to reduction in interzone thickness. (A) Immunohistochemistry with 3C2 (antibody against the viral gag protein) marks the viral infection domain in green. (B-D) represent meta-tarsophalangeal (MTP) joint of the uninfected contralateral control limb and (E-G) represent RCAS-cNFIA RNAi infected meta-tarsophalangeal (MTP) joint region. (B′-D′) are magnified regions from (B-D) and (E′-G′) are magnified regions from (E-G) respectively. RNA *in situ* hybridization images for *COL2A1* (B, B′, E and E′), *PHLDA2* (C, C′, F and F′) and *ChEST302p20* (D, D′, G and G′). (B and B′)

Dotted lines mark the OCL and sandwiched between them is IL. (A), (E), (F) and (G) are serial sections separated by 5µm. Similarly (B-D) are serial sections separated by 5µm. n=5; Scale bar- 100 µm.

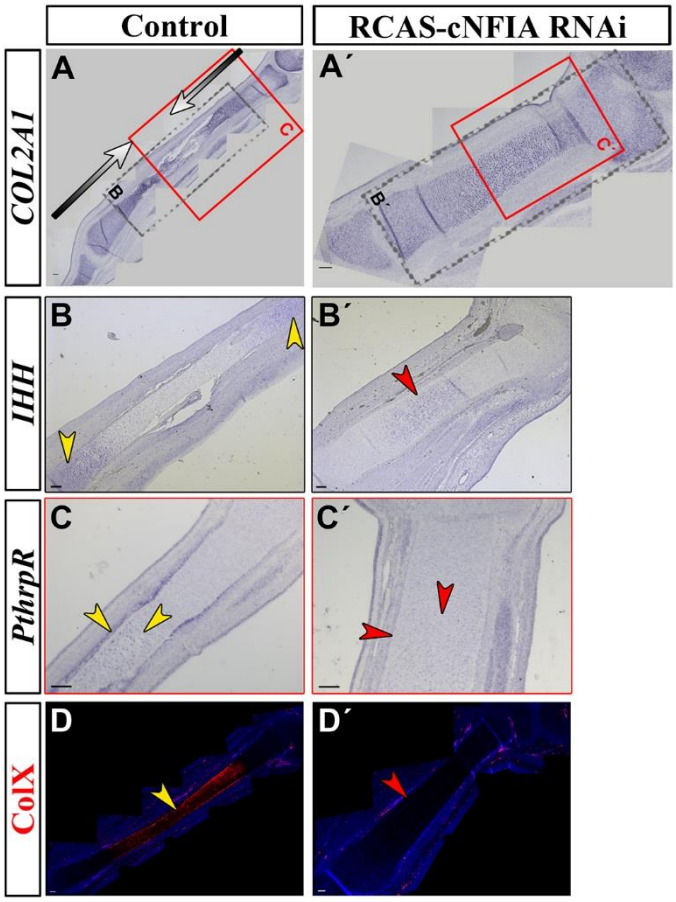

Fig. 2. NFIA loss-of-function blocks the progression of transient cartilage differentiation. (A-D) represent tibia of uninfected contralateral control limb and (A′-D′) represent RCAS-cNFIA RNAi infected tibia element at HH36. RNA *in situ* hybridization images for *COL2A1* (A and A′), *IHH* (B and B′) and *PthrpR* (C and C′). (D and D′) Immunohistochemistry for ColX. The arrows in panel A depict the graded expression of *IHH* which is missing in panel A′. Panels B and B′ represent the regions marked by black dotted boxes in panels A and A′. Panels C and C′ represent the regions marked by red boxes in panels A and A′. Yellow arrowheads in panels B, C and D mark expression domains of *IHH*, *PthrpR* and ColX, respectively while the red arrowheads in panels B′, C′ and D′ mark the down-regulation of these expression levels. n=5; Scale bar- 100 µm.

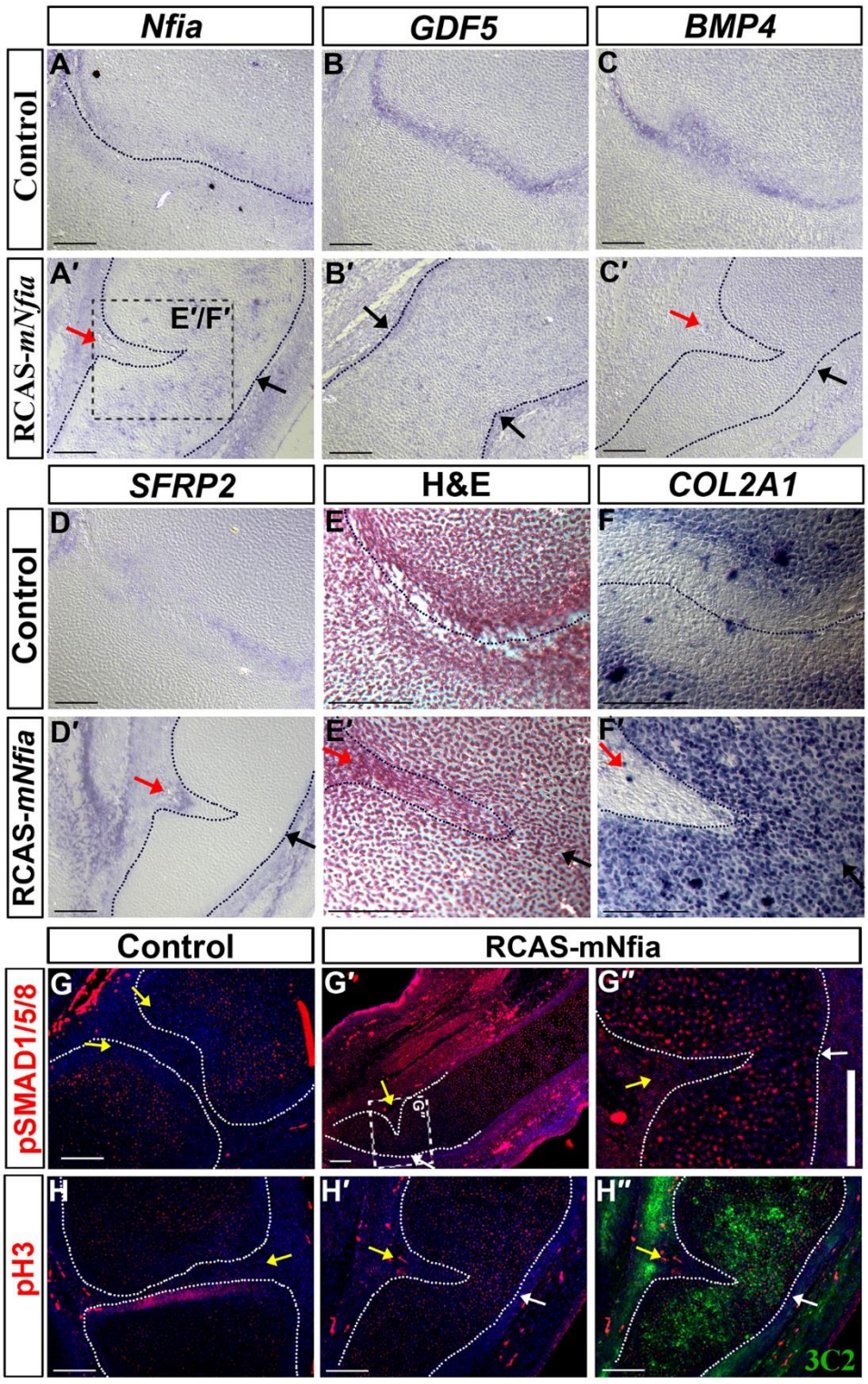

Fig. 3. *Nfia* gain-of-function leads to loss of putative joint site and induces chondrogenesis. (A-H) MTP joint of the uninfected contralateral control limb and (A′-H′) RCAS-m*Nfia* infected MTP joint region at HH36. RNA *in situ* hybridization images for *mNfia* (A and A′), *GDF5* (B and B′), *BMP4* (C and C′), *SFRP2* (D and D′), and *COL2A1* (F

and F′). (E and E′) Haematoxylin and Eosin stained images. (A′-F′) Black arrows mark the absence of putative MTP joint region due to RCAS-m*Nfia* infection while red arrows mark the uninfected MTP joint region within the same element. Panels E′ and F′ correspond to the region marked by a dotted black box in A′. (A′-H′, except B′) are serial sections separated by 5µm. (G and G′) immunohistochemistry for pSMAD1/5/8. (H and H′) immunohistochemistry for phosphohistone H3. (G″) magnified view of the boxed region from (G′). (H″) represents the overlap of infected region (3C2, green) and pH3 immunoreactivity from panel (H′). (G′, H′) White arrows mark the absence of putative MTP joint region due to RCAS-m*Nfia* infection while yellow arrows mark the uninfected MTP joint region within the same element. In uninfected contralateral control (G) yellow arrows mark the absence of pSMAD1/5/8 within interzone and in domain adjacent to interzone region, and in (H) yellow arrows mark the phosphohistoneH3 negative interzone region. (G′, H′) are serial section images separated by 5µm. Skeletal element is outlined via dotted lines. n=6; Scale bar- 100 µm.

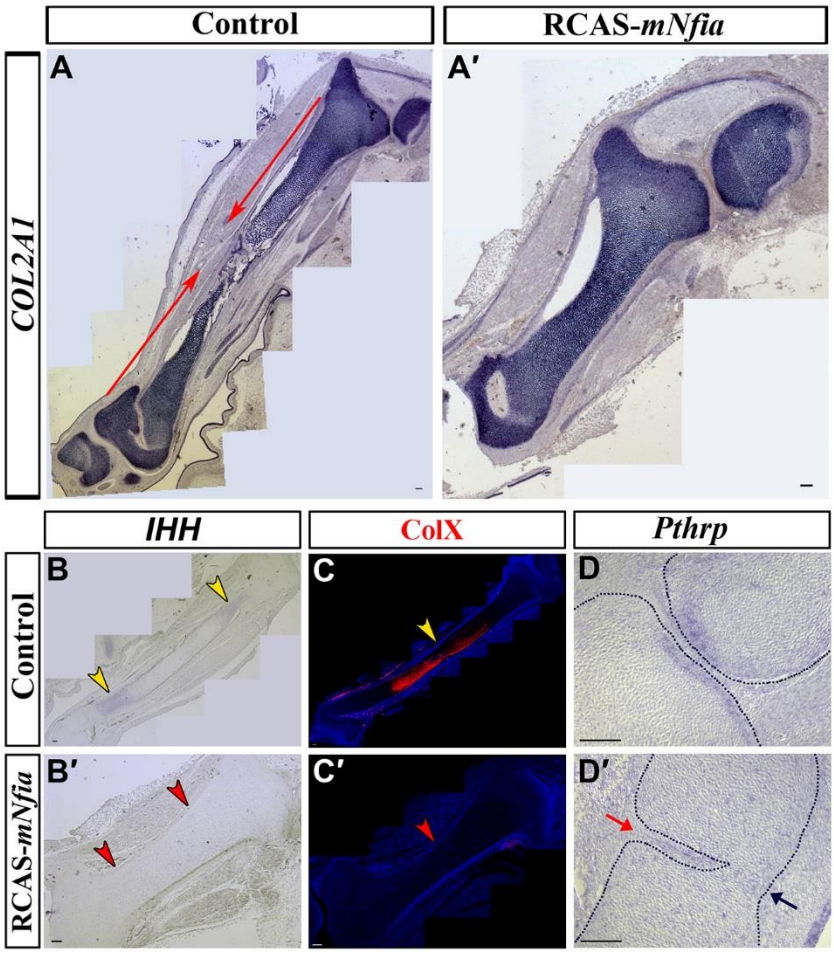

Fig. 4. *Nfia* gain-of-function blocks maturation of transient cartilage cells into pre-hypertrophy and hypertrophy. (A-C) represent tibia of uninfected contralateral control limb and (A′-C′) represent RCAS-m*Nfia* infected tibia element at HH36. (D) MTP joint region of uninfected contralateral control and (D′) RCAS-m*Nfia* infected MTP joint at HH36. RNA *in situ* hybridization images for *COL2A1* (A and A′), *IHH* (B and B′) and *Pthrp* (D and D′). (C and C′) Immunohistochemistry for ColX. (A) Red arrows mark gradual downregulation of *COL2A1* expression from epiphysis to diaphysis as the chondrocytes undergo maturation not apparent in (A′) RCAS-m*Nfia* infected tibia element. Yellow arrows mark the region of (B) *IHH* and (C) ColX expression in control while red arrows mark the absence of (B′) *IHH* and (C′) ColX expression in RCAS-m*Nfia* infected tibia element. (D and D′) Skeletal element is outlined via dotted lines. (D′) Black arrow marks the RCAS-m*Nfia* infected putative MTP joint region while red arrow marks the uninfected MTP joint region

within the same element. (A-C) are serial section images separated by 5µm. (A′-C′) are serial section images separated by 5µm. (D and D′) are serial sections of the specimen used in Fig. 3A′-H′, except B′. n=6; Scale bar- 100 µm.

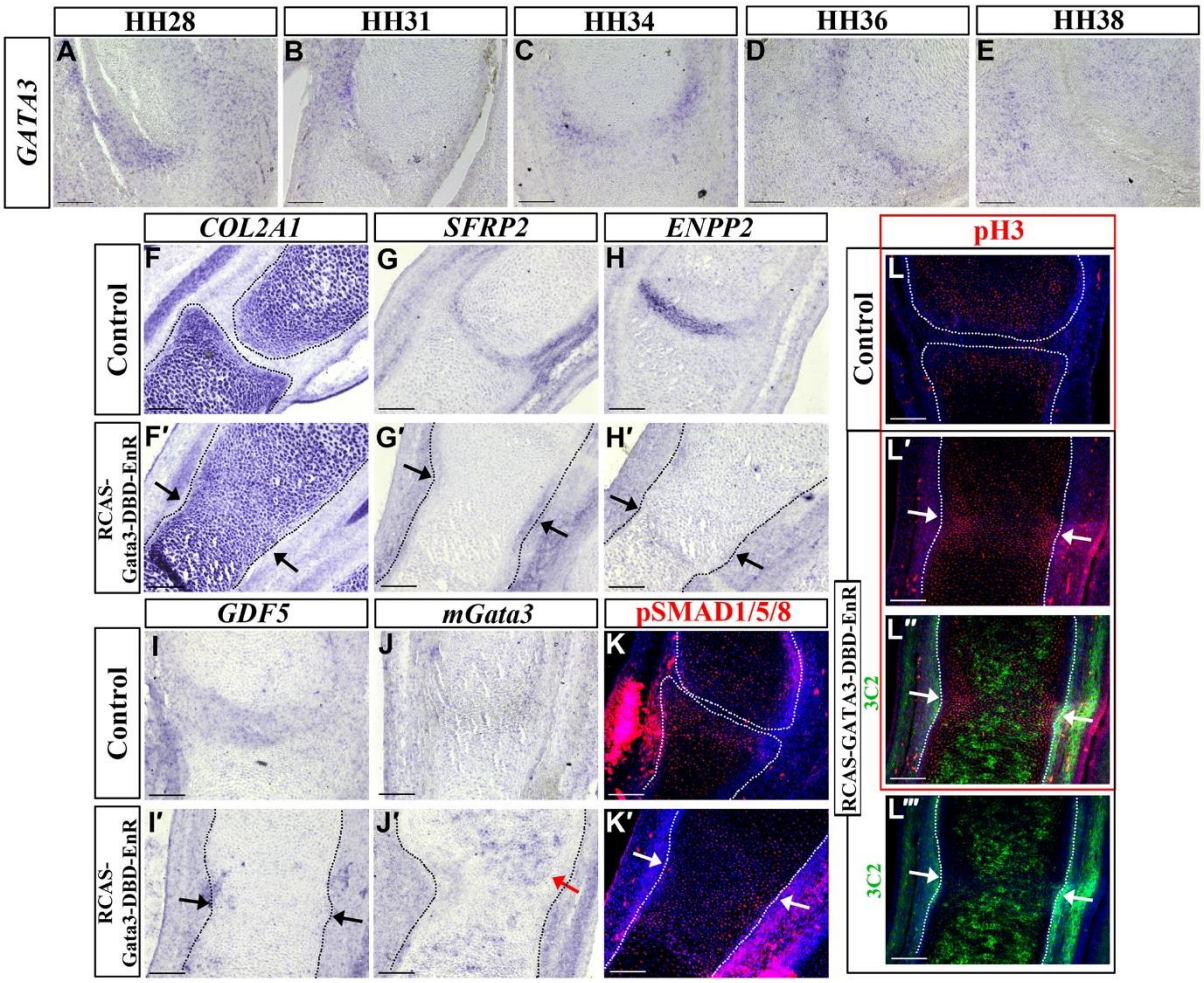

Fig. 5. *GATA3* loss-of-function leads to the loss of putative joint site and induces transient cartilage like fate in the putative joint region. (A-E) RNA *in situ* hybridization images for *GATA3* in chick MTP joint from HH28-HH38. (F-L) MTP joint of the uninfected contralateral control limb and (F′-L′) RCAS-*Gata3*-EnR infected MTP joint region. RNA *in situ* hybridization images for *COL2A1* (F and F′), *SFRP2* (G and G′), *ENPP2* (H and H′), *GDF5* (I and I′) and *mGata3* (J and J′). Black arrows mark the absence of the putative phalangeal joint region due to RCAS-Gata3-EnR infection. (J′) Red arrow marks the expression of *mGata3* across the putative phalangeal joint region. (K and K′) immunohistochemistry for pSMAD1/5/8. (L and L′) immunohistochemistry for phosphohistone H3. (L‴) immunohistochemistry for 3C2 (antibody against viral gag protein).(L″) merged images for L′ and L‴. White arrows mark the loss of the putative

phalangeal joint region due to RCAS-Gata3-EnR infection. (F′-H′ and K′) are serial sections separated by 5µm. Similarly (I′, J′ and L′) are serial sections separated by 5µm. n=7; Scale bar- 100 µm.

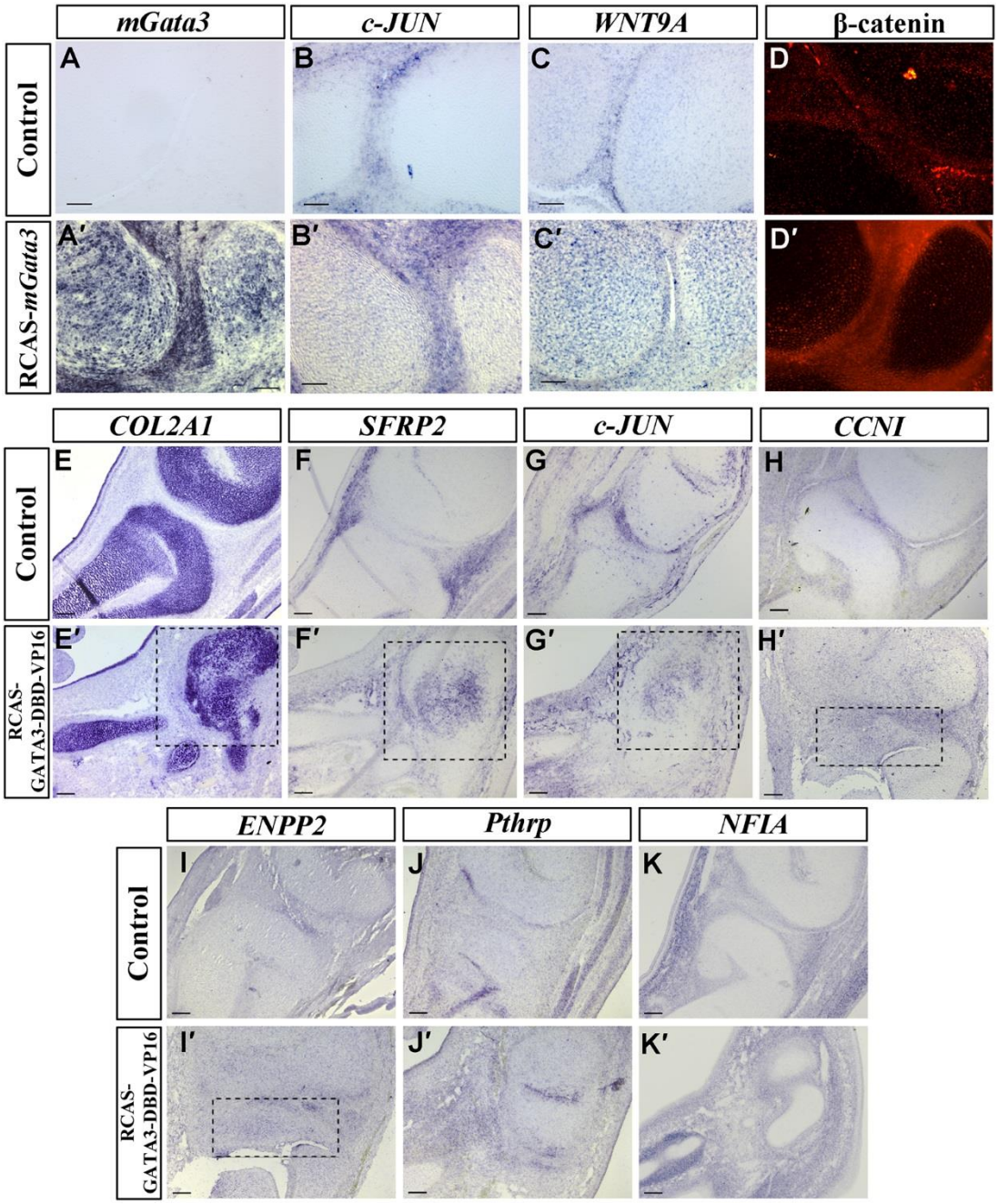

Fig. 6. *Gata3* gain-of-function promotes ectopic expression of articular cartilage markers. (A-D) represent tibio-tarsal joint of an uninfected contralateral control limb and (A′-D′) represent RCAS-*mGata3* infected tibio-tarsal joint region. RNA *in situ* hybridization images for *mGata3* (A and A′), *c-JUN* (B and B′), *WNT9A* (C and C′). (D and D′) immunohistochemistry for β-catenin. (E-K) represent tibio-tarsal joint of an uninfected contralateral control limb and (E′-K′) represent RCAS-*Gata3*-VP16 infected tibio-tarsal joint

region. RNA *in situ* hybridization images for *COL2A1* (E and E′), *SFRP2* (F and F′), *c-JUN* (G and G′), *CCNI* (H and H′), *ENPP2* (I and I′), *Pthrp* (J and J′) and *NFIA* (K and K′). Dotted box in (E′-G′) mark the downregulation of *COL2A1* along with ectopic expression of *SFRP2* and *c-JUN* in similar regions, respectively. While dotted box in (H′-I′) mark ectopic expression of *CCNI* and *ENPP2* in similar regions, respectively. (E′-G′ and J′-K′) are serial sections separated by 5µm. Similarly (H′ and I′) are serial sections separated by 5 µm. For RCAS-*mGata3, n= 4;* For RCAS-*Gata3*-VP16, n=6; Scale bar- 100 µm.

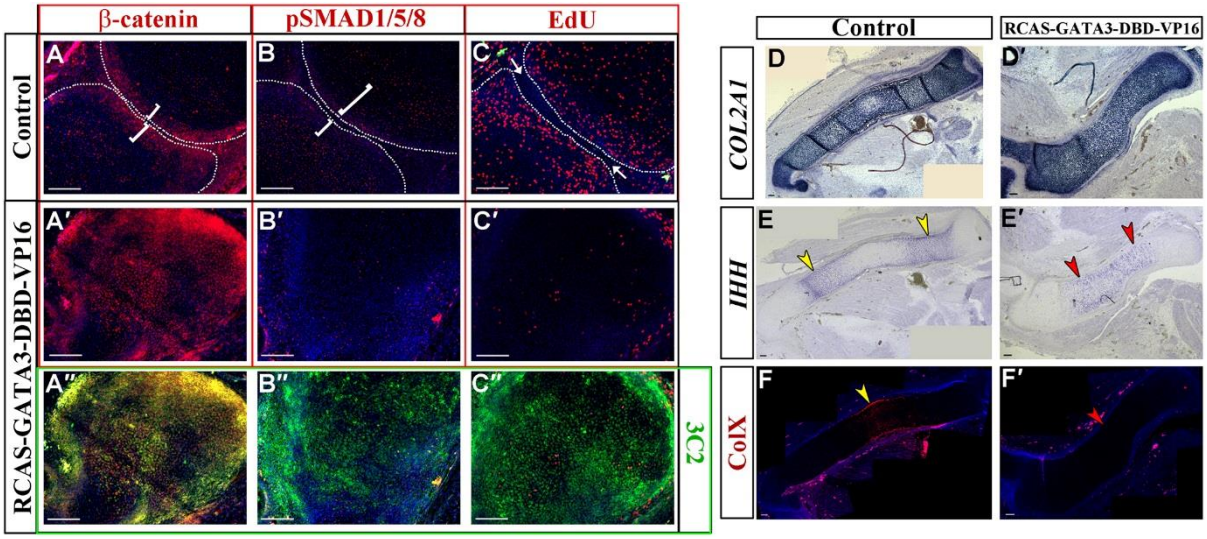

Fig. 7. *Gata3* gain-of-function induces articular cartilage like attributes in putative transient cartilage cells and blocks maturation of transient cartilage cells into hypertrophic state. (A-C) tibio-tarsal joint of the uninfected contralateral control limb and (A′-C′) represent RCAS-Gata3-VP16 infected tibio-tarsal joint region. (A and A′) immunohistochemistry for β-catenin. (B and B′) immunohistochemistry for pSMAD1/5/8. (C and C′) EdU-incorporated cells in red. (A″-C″) Double immunohistochemistry with anti-β-catenin (A″), anti-pSMAD1/5/8 (B″), and EdU-incorporated cells (C″) in red and 3C2 (antibody against viral gag protein) in green. (A′-C′) are magnified images of a similar region represented by the dotted boxed in Fig. 6E′-G′. Dotted lines mark the interzone region. (A′-C′) are serial section images separated by 5µm. Square brackets mark the chondrogenous layers adjacent to the joint line positive for β-catenin but absent for pSMAD1/5/8. Arrows indicate the joint line deficient of proliferative cells. (D-F) represent femur of uninfected contralateral control limb and (D′-F′) represent RCAS-*Gata3*-VP16 infected femur. RNA *in situ* hybridization images for *COL2A1* (D and D′) and *IHH* (E and E′). (F and F′) Immunohistochemistry for ColX. (D-F) are serial section images separated by 5µm. Similarly (D′-F′) are serial section images separated by 5µm. Yellow arrowheads in panels E and F mark expression domains of *IHH* and ColX, respectively while the red arrowheads in panels

E′ and F′ mark the down-regulation of these expression levels. For RCAS-*Gata3*-VP16, n=6; Scale bar- 100 µm.

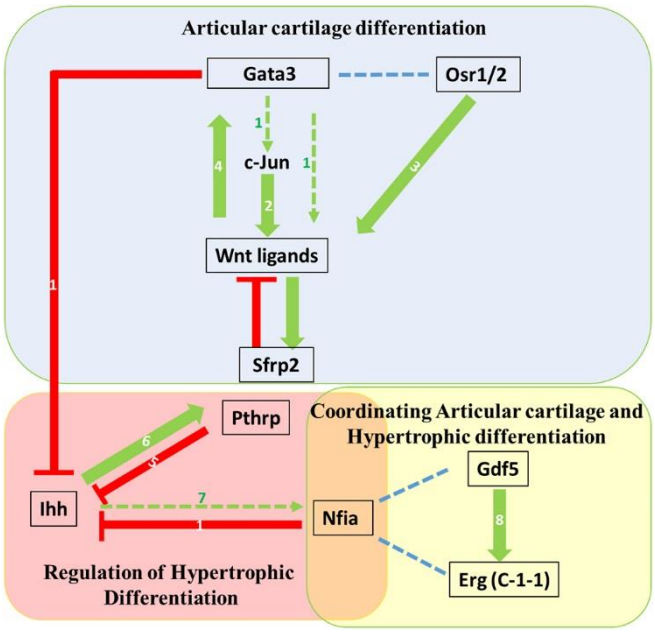

Fig. 8. Speculative model of involvement of *Gata3* and *Nfia* in Articular cartilage. Arrows with solid lines indicate demonstrated functional interaction (either in this study or in the published literature) while arrows with dashed lines indicate predicted regulation. Dashed blue lines indicate possible functional interaction of unspecified nature. The numbers indicate the source of information. 1 = this study; 2 = (Kan and Tabin, 2013); 3 = (Gao et al., 2011); 4 = (Grote et al., 2008); 5 = (Lanske et al., 1996); 6 =(Vortkamp et al., 1996); 7 = (Genovesi et al., 2013); 8 = (Iwamoto et al., 2007).

SUPPLEMENTARY FIGURES

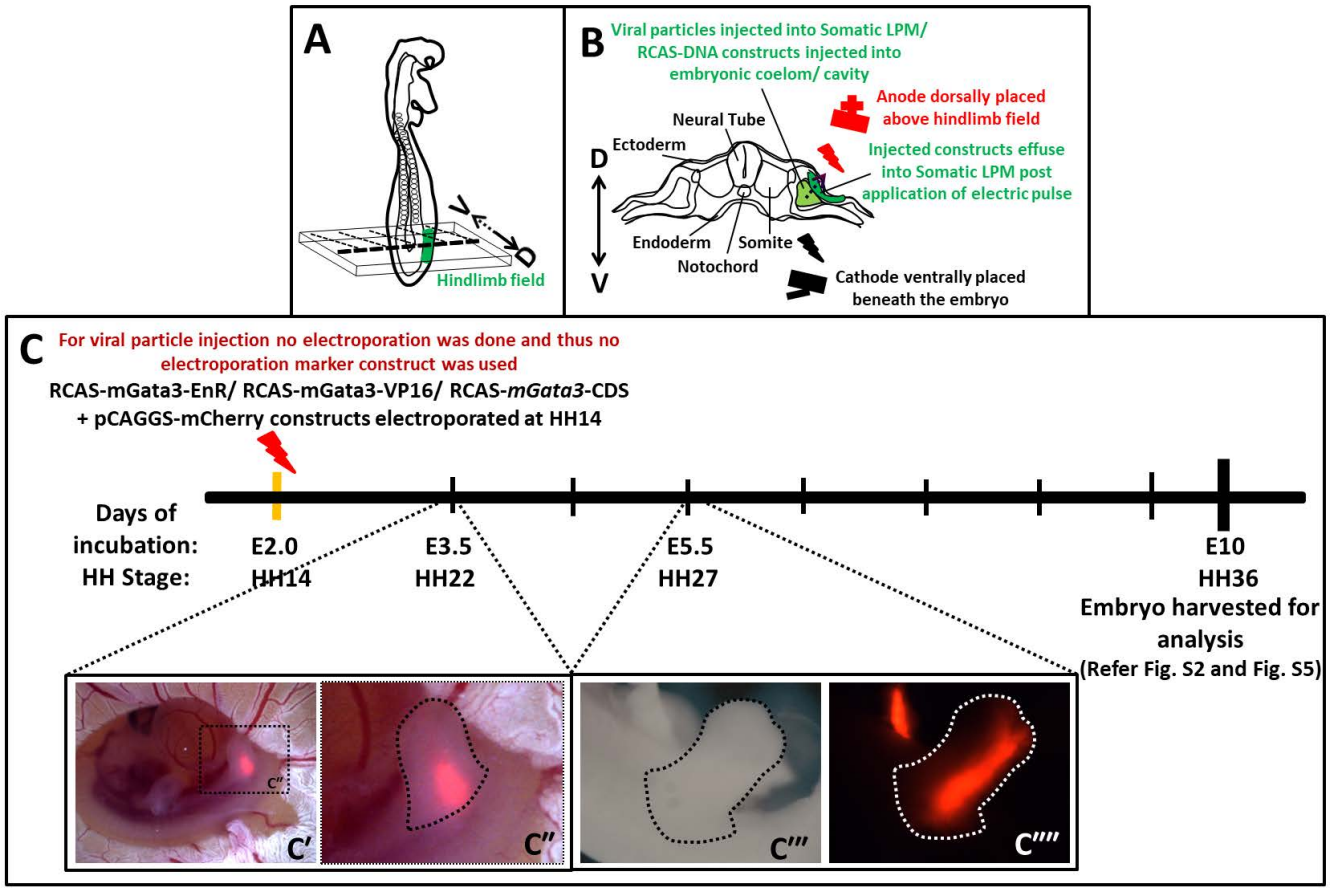

Fig. S1. Schematic representation of the experiments carried out in this study. (A) In a HH14 stage chick embryo limb fields are recognized as small protuberances at specific locations along the body wall of the embryo or LPM (lateral plate mesoderm). Hindlimb field is marked in green. (B) A transverse section of the limb field represented in (A) along the dorso-ventral (D-V) axis. At stage HH14 the DNA constructs or retroviral particles, mixed with 0.1% fast green, was injected into the embryonic space between the somatic LPM and splanchnic LPM at a concentration of 2µg/µl using a microinjector. Post-microinjection electroporation is performed if DNA construct was injected. As soon as the DNA was injected platinum cathode was placed within the albumin beneath the yolk sac while an L-shaped anode was placed in parallel to the embryo over the hindlimb field before electric pulses (10V, 50ms pulse-on, 950ms pulse-off, five repetitions) were applied. Injected constructs get inside the nucleus of the cells on the dorsal side of the LPM, called the somatic LPM which eventually gives rise to limb buds as represented in (C″). (C) Timeline of the experimental setup. At stage HH14 RCAS construct RCAS-*mGata3*-CDS or RCAS-GATA3DBD-VP16 or RCAS-GATA3DBD-EnR mixed with 0.5µg/µl pCAGGS-mCherry was electroporated as represented in panel (B). (C′) At stage HH22 expression of mCherry within the limb bud indicates successful electroporation. (C″) Magnified image of the hindlimb region marked in (C′) represents the mCherry expression within the limb bud. (C‴) represents mCherry expression at day5.5 i.e. HH27. (C‴) is the bright-filed image of the same limb bud. All the embryos analysed in this study were harvested at HH36.

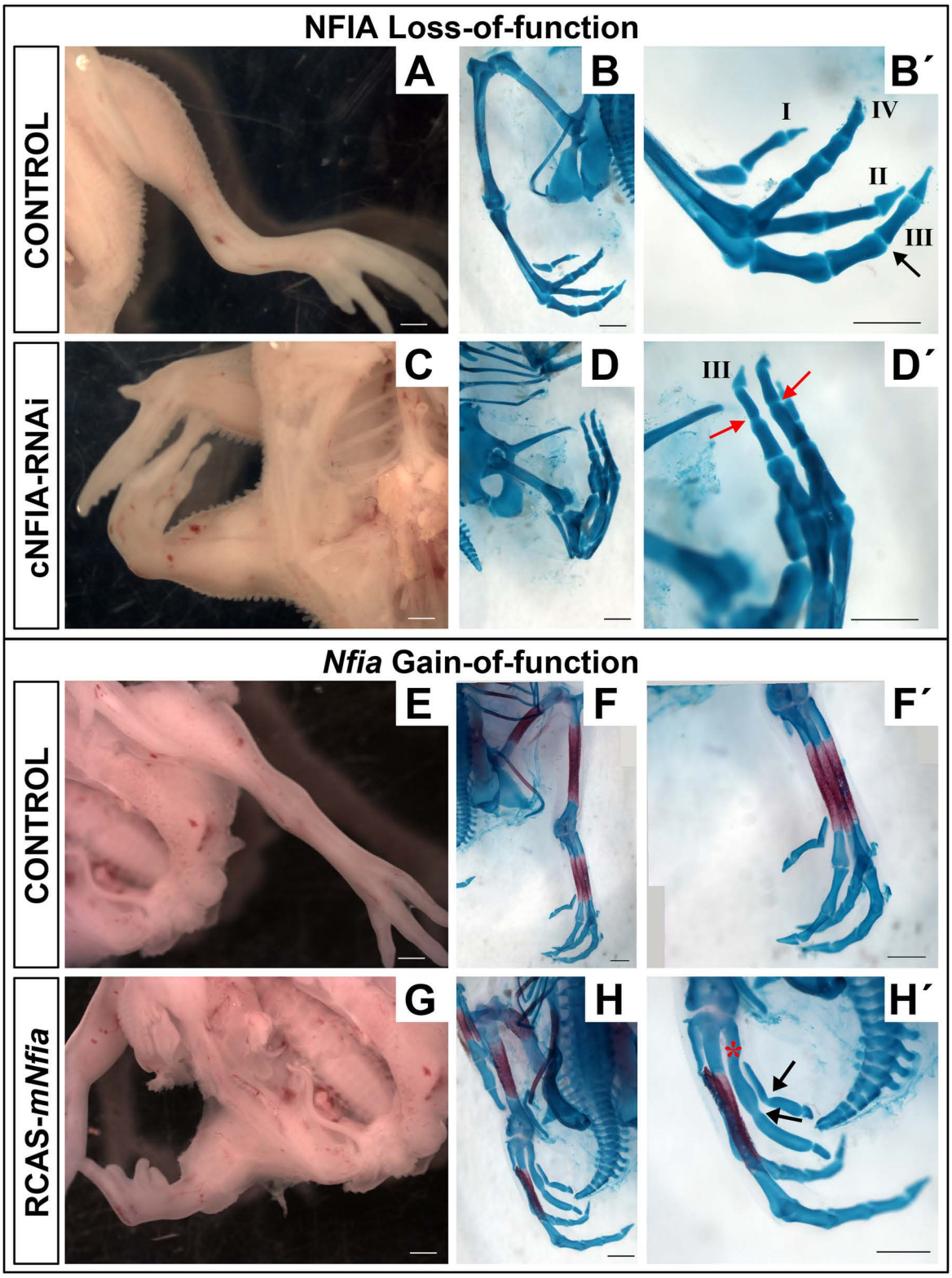

Fig. S2. Skeletal prep analysis of RCAS-cNFIARNAi and RCAS-m*Nfia* infected limbs compared to respective uninfected contralateral control limbs. Whole mount view of unfixed, unstained RCAS-cNFIARNAi infected limb (C) compared with uninfected contralateral control (A) at HH36. (B) Alcian blue stained uninfected contralateral control limb, (B′) shows magnified view of the phalangeal region where black arrow marks the segmented joint between the second and the third phalanx in the third digit. (D) Alcian blue stained RCAS-cNFIA-shRNAi infected limb, (D′) shows magnified view of the phalangeal region where red arrow marks the unsegmented joint between the second and the third phalanx in the third digit. Whole mount view of unfixed, unstained RCAS-m*Nfia* infected limb (G) compared with uninfected contralateral control (E) at HH36. (F) Alcian blue-alizarin red stained uninfected contralateral control limb and (F′) shows magnified view of the meta-tarsus. (H) Alcian blue-alizarin red stained RCAS-m*Nfia* infected limb and (H′) shows magnified view of the meta-tarsus, arrows marks the unsegmented skeletal elements, red asterisk marks the element showing reduced alizarin red staining. Scale bar- 1mm.

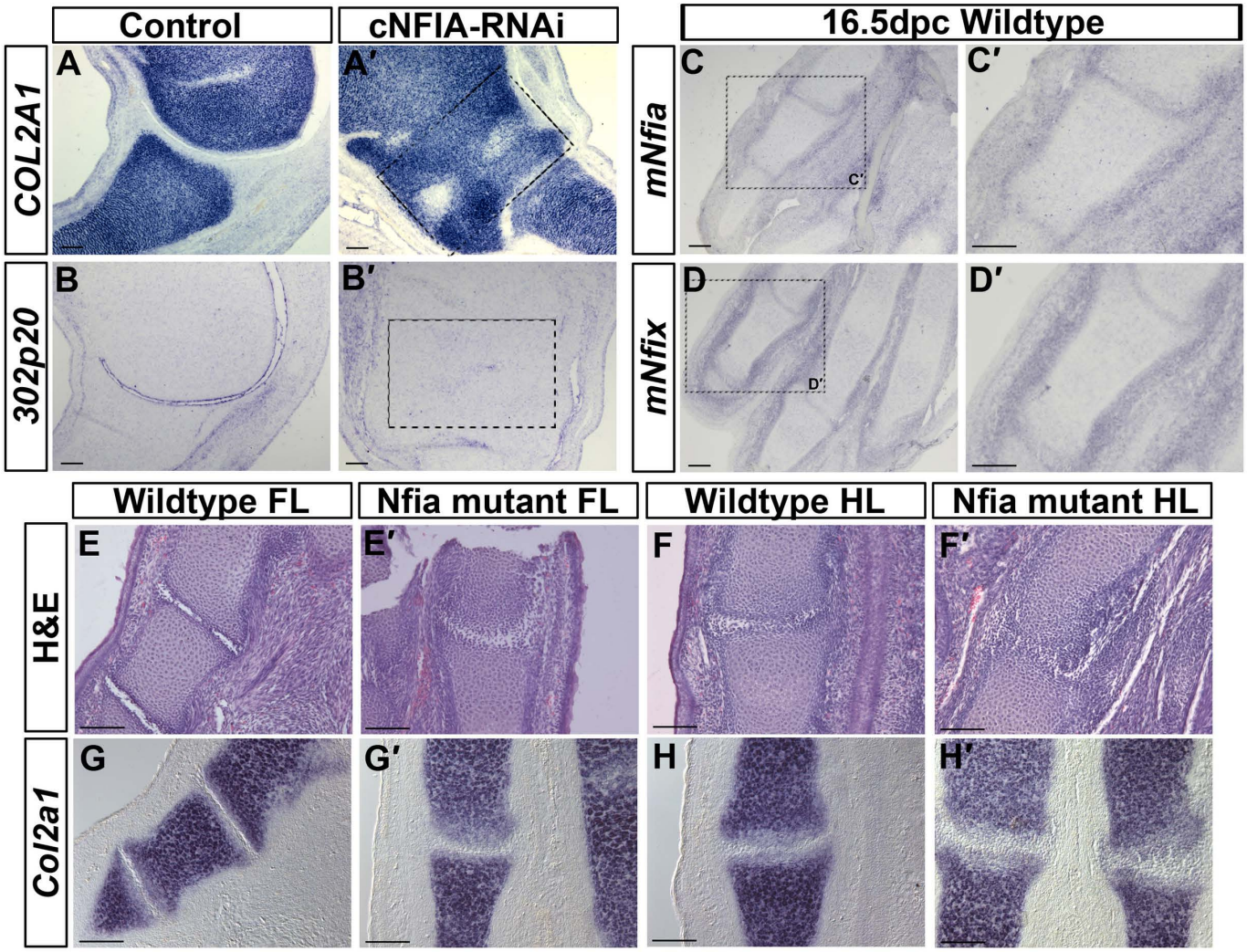

Fig. S3.NFIA loss-of-function leads to loss of interzone markers. (A,B) represent tibio-tarsal joint of an uninfected contralateral control limb and (A′,B′) represent RCAS-*cNFIA-RNAi* infected tibio-tarsal joint region. RNA *in situ* hybridization images for *COL2A1* (A and A′), *ChEST302p20* (B and B′). (C and D) RNA *in situ* hybridization images for*m Nfia* and *mNfix* respectively, (C′ and D′) shows magnified region from (C and D). (E-H) MTP joint of WT control and (E′-H′) *Nfia* mutant limbs. (E, E′, F and F′) Hematoxylin and Eosin staining. (G, G′, H and H′) RNA *in situ* hybridization for mouse *Col2a1*.Scale bar- 100 µm.

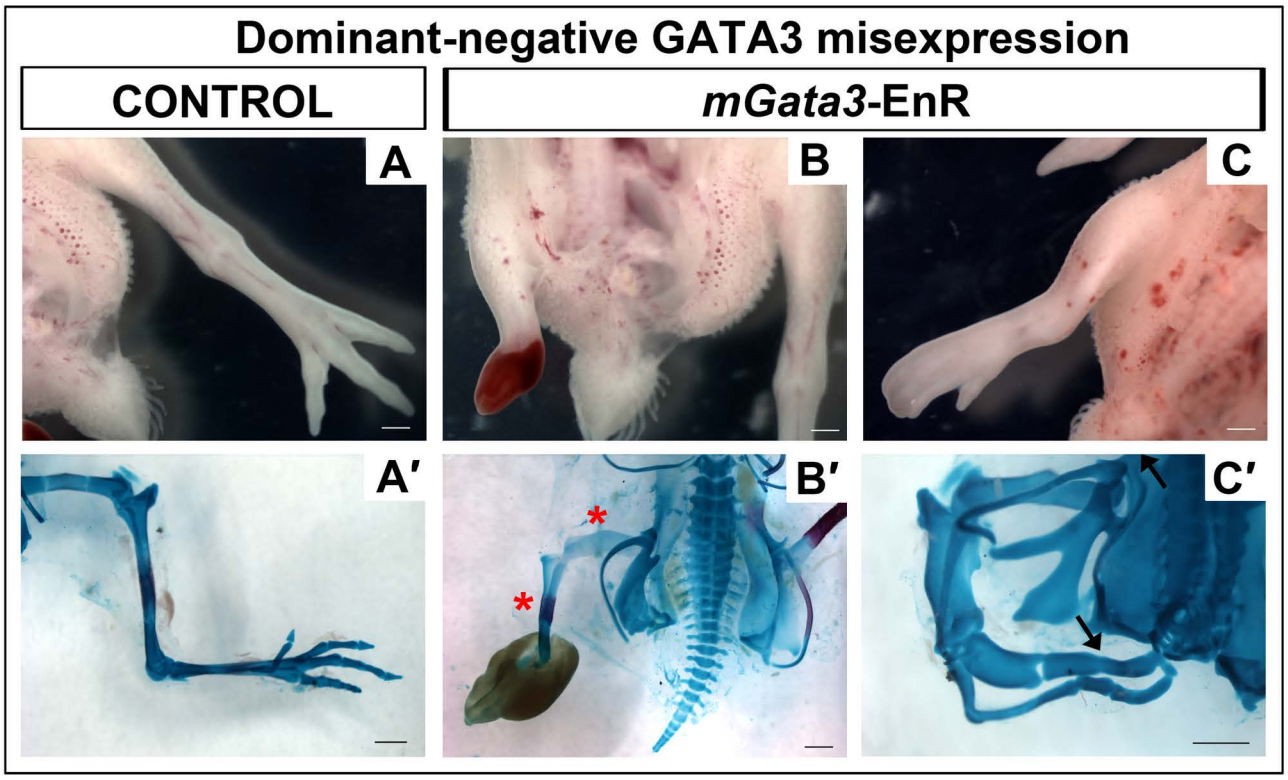

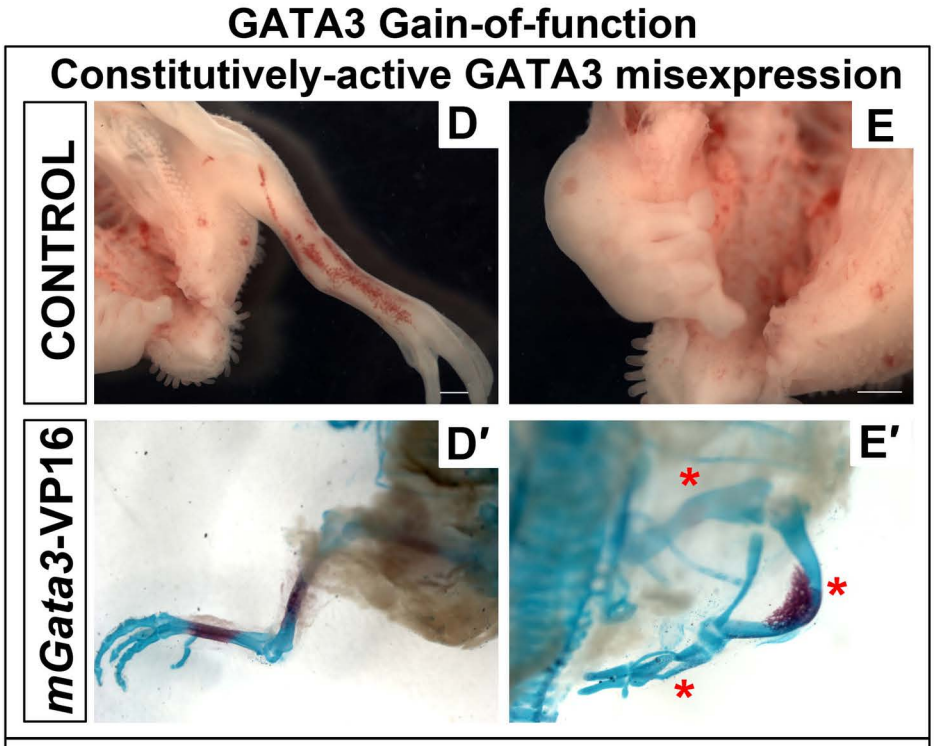

Fig. S4. Strategy adopted for generation of Gata3 gain-of-function and loss-of-function constructs. (A) Represents a full length mouse-GATA3 protein comprising of two amino-terminal transactivation domains followed by two zinc finger domains. (B) GATA3-DBD-V16 represents a constitutively active form of GATA3 generated by fusion of an in-frame strong trans-activator VP16 at the C-terminus of mGATA3 DNA binding domain. Thus constitutively transcribing the genes modulated by GATA3 binding. (C) GATA3-DBD-EnR represents a constitutively active form of GATA3 generated by fusion of an in-frame strong repressor EnR at the C-terminus of mGATA3 DNA binding domain. Thus constitutively repressing the genes modulated by GATA3 binding. The constructs were made as per method described by Kamei et. al. (Kamei et al., 2011)

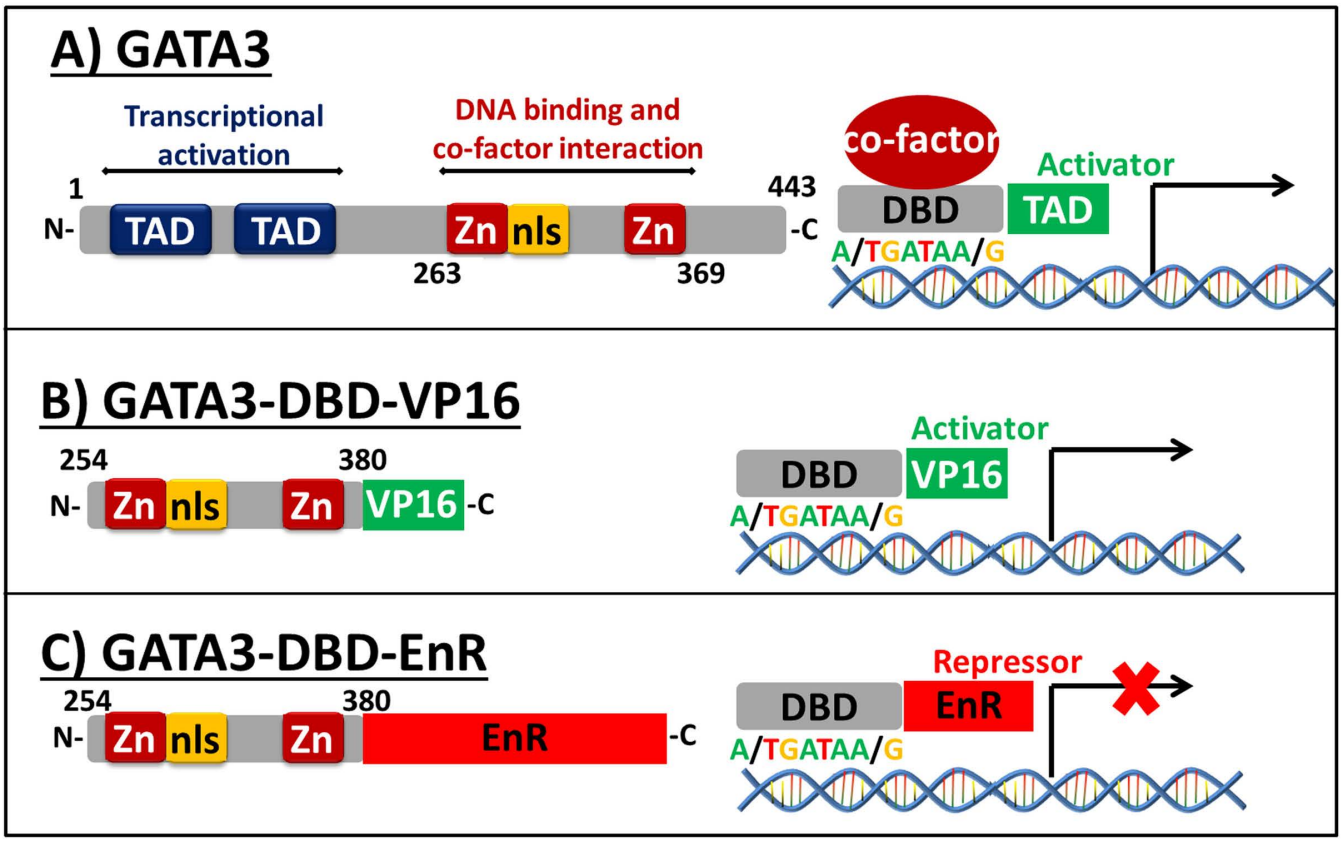

Fig. S5. *Gata3*-EnR and *Gata3*-VP16 infected limbs compared to respective uninfected contralateral control limbs. Whole mount view of unfixed, unstained RCAS-*Gata3*-EnR infected limb (B and C) and uninfected contralateral limb (A) at HH36. Alcian blue-alizarin red stained uninfected contralateral control limb (A′) and RCAS-*Gata3*-EnR infected limb with severe (B′) to less severe (C′) skeletal deformity. Arrows mark the unsegmented skeletal elements; red asterisks mark the elements showing reduced alizarin red staining. Whole mount view of unfixed, unstained RCAS-*Gata3*-VP16 infected limb (E) and uninfected contralateral limb (D) at HH36. Alcian blue-alizarin red stained whole mount skeletons from (D′) uninfected contralateral control limb and (E′) RCAS-*Gata3*-VP16 infected limb, where red asterisks mark the elements showing reduced alizarin red staining. Scale bar- 1mm.

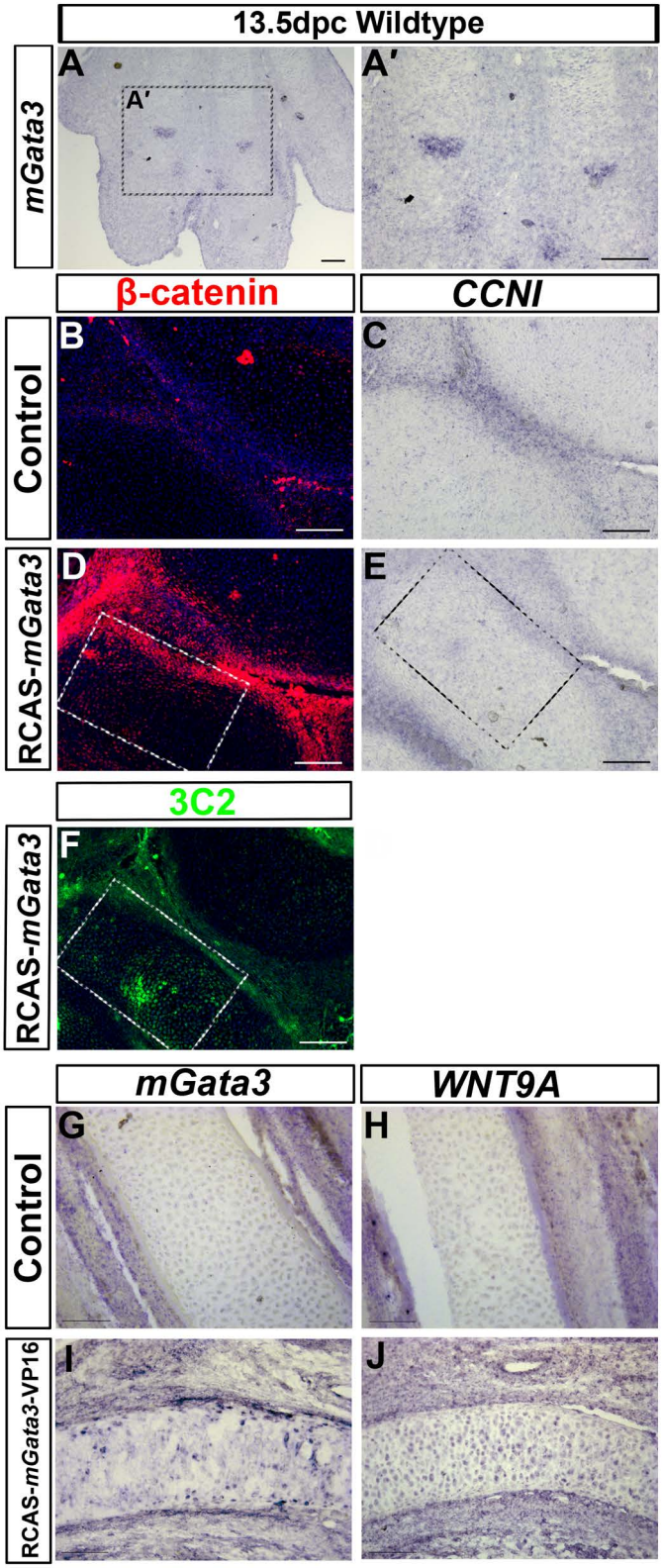

Fig. S6. Gata3 gain-of-function. (A) Expression of mouse *Gata3* mRNA in 13.5dpc mouse hindlimb digits. (A′) Magnified view of the boxed region in Panel A. (B-F) CCNI, an articular cartilage specific gene, is not overexpressed when mGata3 is virally misexpressed. (B and C) represent endogenous level of β-catenin immuno-reactivity (B) and CCNI mRNA expression (C) in tibio-tarsal joint of an uninfected contralateral control chick limb. (D and E) β-catenin immuno-reactivity (D), and CCNI mRNA expression (E), in the RCAS-m*Gata3*-cDNA infected HH36 tibio-tarsal joint region. (F) Immunohistochemistry with 3C2 (antibody against the viral gag protein) on a section serial to the ones used in panels D and E marks the viral infection domain in green within the boxed region. (G-J) Overexpression of mGata3-VP16 causes ectopic expression of Wnt9a. (G) RNA *in situ* hybridization against *mGata3* in non-infected contralateral control tibia. (H) RNA *in situ* hybridization against *WNT9A* in non-infected contralateral control tibia. (I) RNA *in situ* hybridization against mGata3 highlights the mGata3-VP16 infected tibia. (J) Ectopic expression of Wnt9a in the mGata3-VP16 infected tibia. I and J are serial sections. Scale bar- 100 µm.

Supplementary Table S1

Supplementary table 1: Articular cartilage specific genes that were identified as transcriptional targets of Gata3 in the microarray profiling performed by Kourous-Mehr et al. (Kouros-Mehr et al., 2006).

ID_REF	VALUE	Avalue	Description	Symbol
22436	3.019	9.499	ectonucleotide pyrophosphatase/phosphodiesterase 2 (Atx)	Enpp2
36565	1.904	9.611	cyclin I	CCNI
11991	1.364	8.416	hypoxia inducible factor 1, alpha subunit	HIF1A
29726	1.112	9.046	cadherin 11	CDH11
14359	0.889	10.04	fibulin 1	FBLN1
18280	0.685	8.686	tenascin C	TNC
7418	0.412	12.638	growth differentiation factor 5	GDF5
13997	0.384	9.399	chordin	CHRD
12648	0.356	15.331	insulin-like growth factor binding protein 4	IGFBP4
12398	0.351	11.785	wingless-type MMTV integration site 9A	Wnt9a
31109	0.268	10.412	secreted frizzled-related sequence protein 2	SFRP2
27708	0.226	15.643	clusterin	CLU
13437	0.214	11.113	chondroitin sulfate proteoglycan 2 (versican)	CSPG2
35186	0.189	10.053	nuclear factor I/A	NFIA
14761	0.07	8.062	GLI-Kruppel family member GLI3	GLI3
8289	0.016	12.726	catenin (cadherin associated protein), beta 1, 88kDa	CTNNB1

#ID_REF = Unique Identifier
#VALUE = Lowess M Log Ratio (F635 Median, F532 Median), $\log_2$(Het /Null) where Het = fluorescence intensity of WAP-rtTA-Cre;GATA-3$^{flox/+}$sample and Null = fluorescence intensity of WAP-rtTA-Cre;GATA-3$^{flox/flox}$ sample
#Avalue = Lowess A Log Ratio (F635 Median, F532 Median)

Supplementary Data 2: List of clones used

Genes	**ChEST ID/ Source**
SFRP2	ChEST712d9
Atx	ChEST520a5
c-Jun	ChEST520g15
ERG	Cloned
PTHRP	Minina et al., 2001
NFIA *Nuclear factor I/A*	ChEST864l9
mNFIA	Deneen et al., 2006
mNFIX	IRAV 3491917
mGATA3	Kamei et al.,2011
PHLDA2 *Pleckstrin homology-like domain, family A, member 2*	ChEST533e11
Finished cDNA clone ChEST302p20	ChEST302p20
CCNI *Cyclin I*	ChEST605d20
GDF5	Hartmann et al., 2001
BMP4	Francis et al., 1994
COL2A1	Hartmann et al., 2001

mCOL2A1	
WNT9a	ChEST592n13
GATA3	ChEST663o17
IHH	Minina et al., 2001
PTHrPR	Minina et al., 2001

Hartmann C, Tabin CJ. 2001. Wnt-14 plays a pivotal role in inducing synovial joint formation in the developing appendicular skeleton. Cell 104:341-351.

Minina E, Wenzel HM, Kreschel C, Karp S, Gaffield W, McMahon AP, Vortkamp A. 2001. BMP and Ihh/PTHrP signaling interact to coordinate chondrocyte proliferation and differentiation. Development 128:4523-4534.

Kamei, C. N., Kempf, H., Yelin, R., Daoud, G., James, R. G., Lassar, A. B., Tabin, C. J., and Schultheiss, T. M. (2011). Promotion of avian endothelial cell differentiation by GATA transcription factors. Dev Biol *353*, 29-37.

Deneen, B., Ho, R., Lukaszewicz, A., Hochstim, C. J., Gronostajski, R. M., and Anderson, D. J. (2006). The transcription factor NFIA controls the onset of gliogenesis in the developing spinal cord. Neuron *52*, 953-968.

Francis PH, Richardson MK, Brickell PM, Tickle C. 1994. Bone morphogenetic proteins and a signalling pathway that controls patterning in the developing chick limb. Development 120:209-218.

SUPPLEMENTARY FIGURES

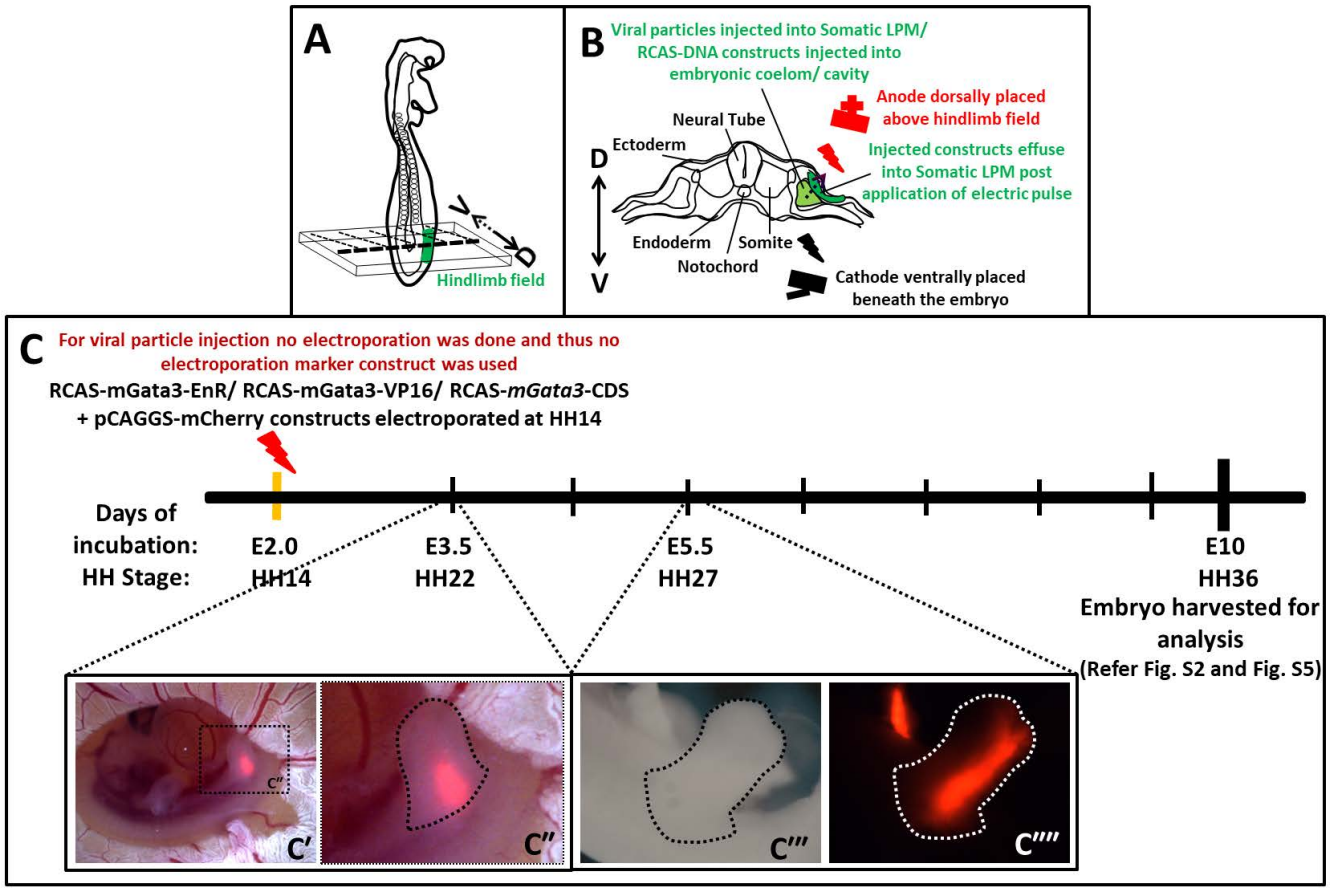

Fig. S1. Schematic representation of the experiments carried out in this study. (A) In a HH14 stage chick embryo limb fields are recognized as small protuberances at specific locations along the body wall of the embryo or LPM (lateral plate mesoderm). Hindlimb field is marked in green. (B) A transverse section of the limb field represented in (A) along the dorso-ventral (D-V) axis. At stage HH14 the DNA constructs or retroviral particles, mixed with 0.1% fast green, was injected into the embryonic space between the somatic LPM and splanchnic LPM at a concentration of 2µg/µl using a microinjector. Post-microinjection electroporation is performed if DNA construct was injected. As soon as the DNA was injected platinum cathode was placed within the albumin beneath the yolk sac while an L-shaped anode was placed in parallel to the embryo over the hindlimb field before electric pulses (10V, 50ms pulse-on, 950ms pulse-off, five repetitions) were applied. Injected constructs get inside the nucleus of the cells on the dorsal side of the LPM, called the somatic LPM which eventually gives rise to limb buds as represented in (C″). (C) Timeline of the experimental setup. At stage HH14 RCAS construct RCAS-*mGata3*-CDS or RCAS-GATA3DBD-VP16 or RCAS-GATA3DBD-EnR mixed with 0.5µg/µl pCAGGS-mCherry was electroporated as represented in panel (B). (C′) At stage HH22 expression of mCherry within the limb bud indicates successful electroporation. (C″) Magnified image of the hindlimb region marked in (C′) represents the mCherry expression within the limb bud. (C‴) represents mCherry expression at day5.5 i.e. HH27. (C‴) is the bright-filed image of the same limb bud. All the embryos analysed in this study were harvested at HH36.

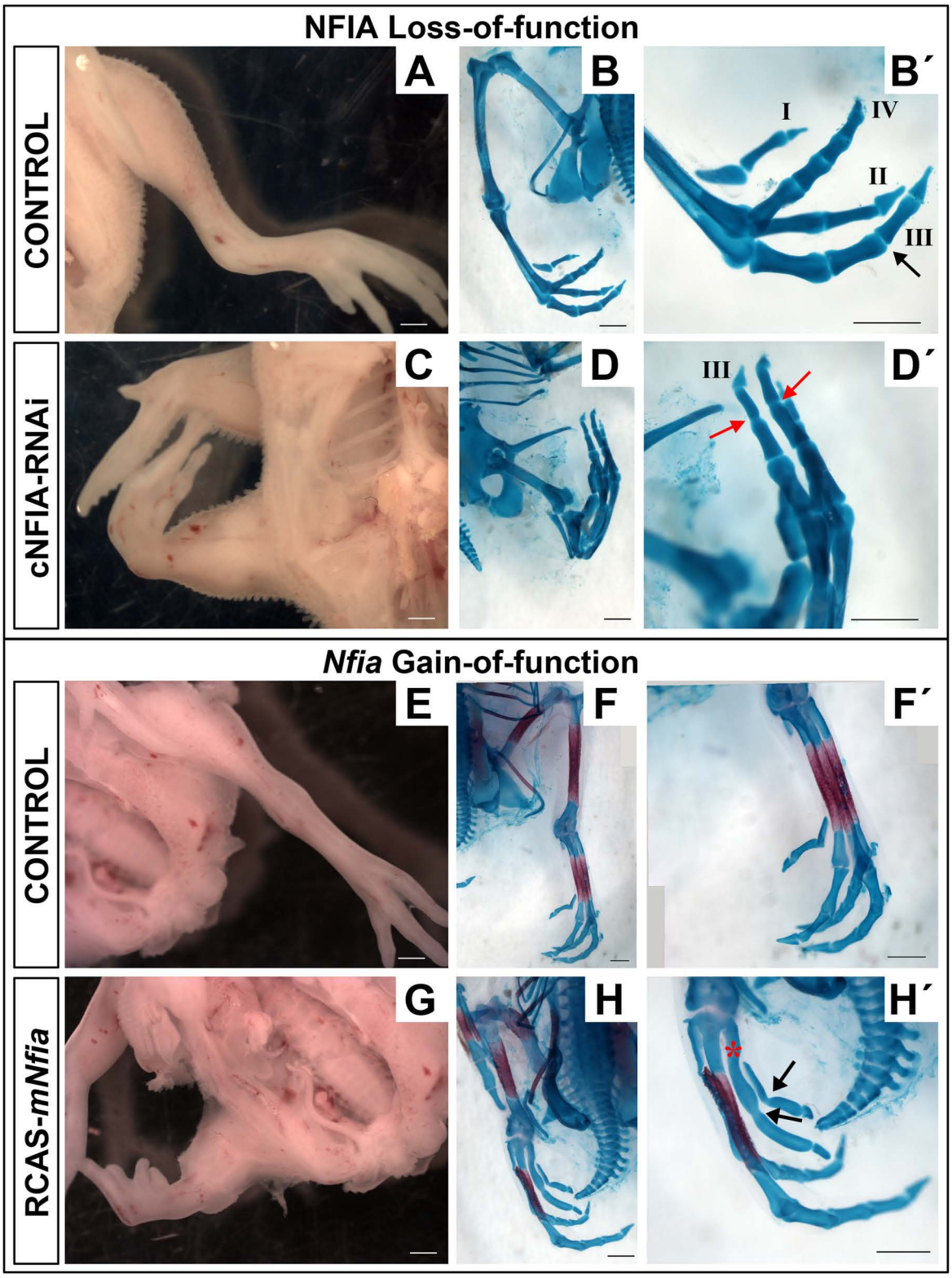

Fig. S2. Skeletal prep analysis of RCAS-cNFIARNAi and RCAS-m*Nfia* infected limbs compared to respective uninfected contralateral control limbs. Whole mount view of unfixed, unstained RCAS-cNFIARNAi infected limb (C) compared with uninfected contralateral control (A) at HH36. (B) Alcian blue stained uninfected contralateral control limb, (B′) shows magnified view of the phalangeal region where black arrow marks the segmented joint between the second and the third phalanx in the third digit. (D) Alcian blue stained RCAS-cNFIA-shRNAi infected limb, (D′) shows magnified view of the phalangeal region where red arrow marks the unsegmented joint between the second and the third phalanx in the third digit. Whole mount view of unfixed, unstained RCAS-m*Nfia* infected limb (G) compared with uninfected contralateral control (E) at HH36. (F) Alcian blue-alizarin red stained uninfected contralateral control limb and (F′) shows magnified view of the meta-tarsus. (H) Alcian blue-alizarin red stained RCAS-m*Nfia* infected limb and (H′) shows magnified view of the meta-tarsus, arrows marks the unsegmented skeletal elements, red asterisk marks the element showing reduced alizarin red staining. Scale bar- 1mm.

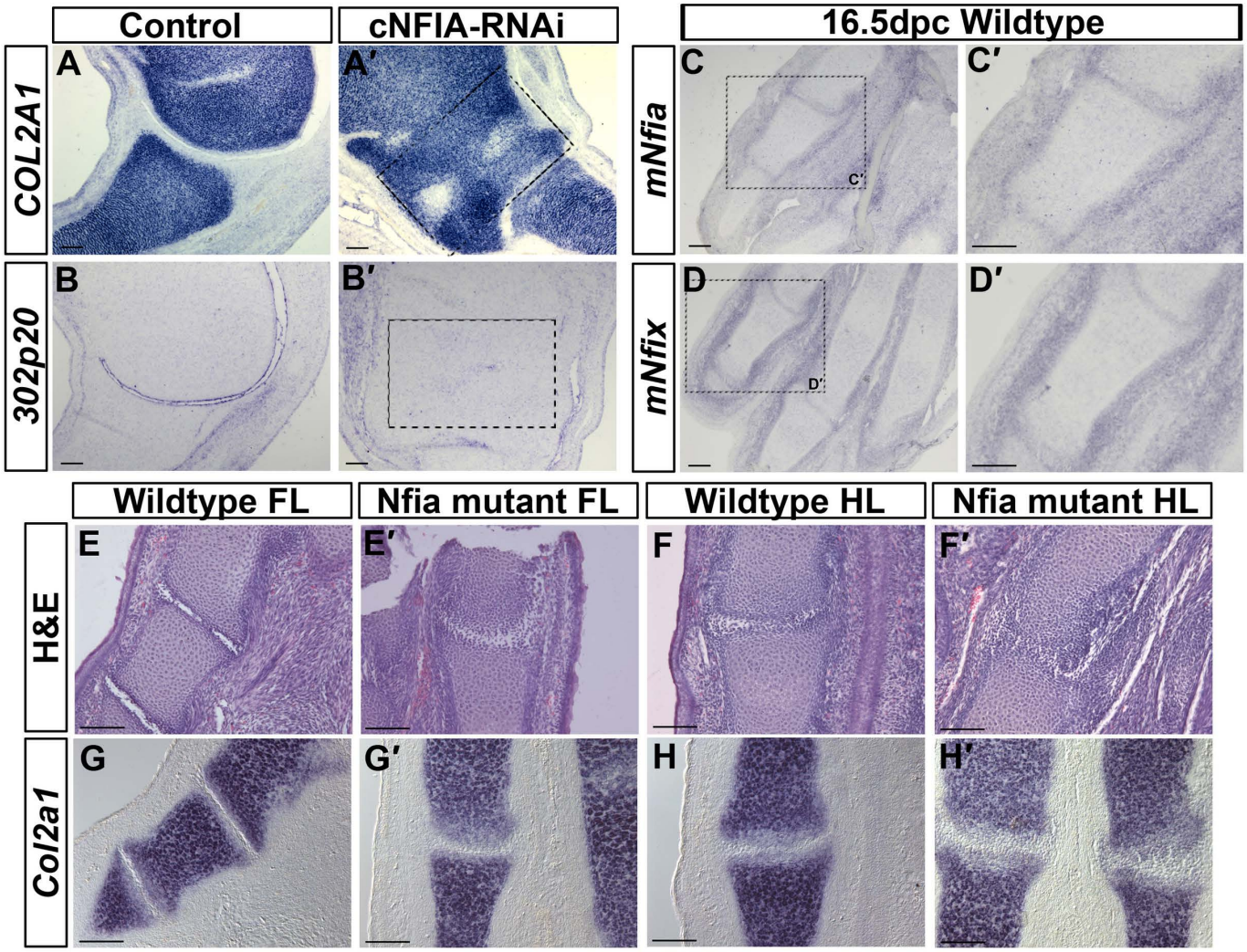

Fig. S3.NFIA loss-of-function leads to loss of interzone markers. (A,B) represent tibio-tarsal joint of an uninfected contralateral control limb and (A′,B′) represent RCAS-*cNFIA-RNAi* infected tibio-tarsal joint region. RNA *in situ* hybridization images for *COL2A1* (A and A′), *ChEST302p20* (B and B′). (C and D) RNA *in situ* hybridization images for*m Nfia* and *mNfix* respectively, (C′ and D′) shows magnified region from (C and D). (E-H) MTP joint of WT control and (E′-H′) *Nfia* mutant limbs. (E, E′, F and F′) Hematoxylin and Eosin staining. (G, G′, H and H′) RNA *in situ* hybridization for mouse *Col2a1*.Scale bar- 100 µm.

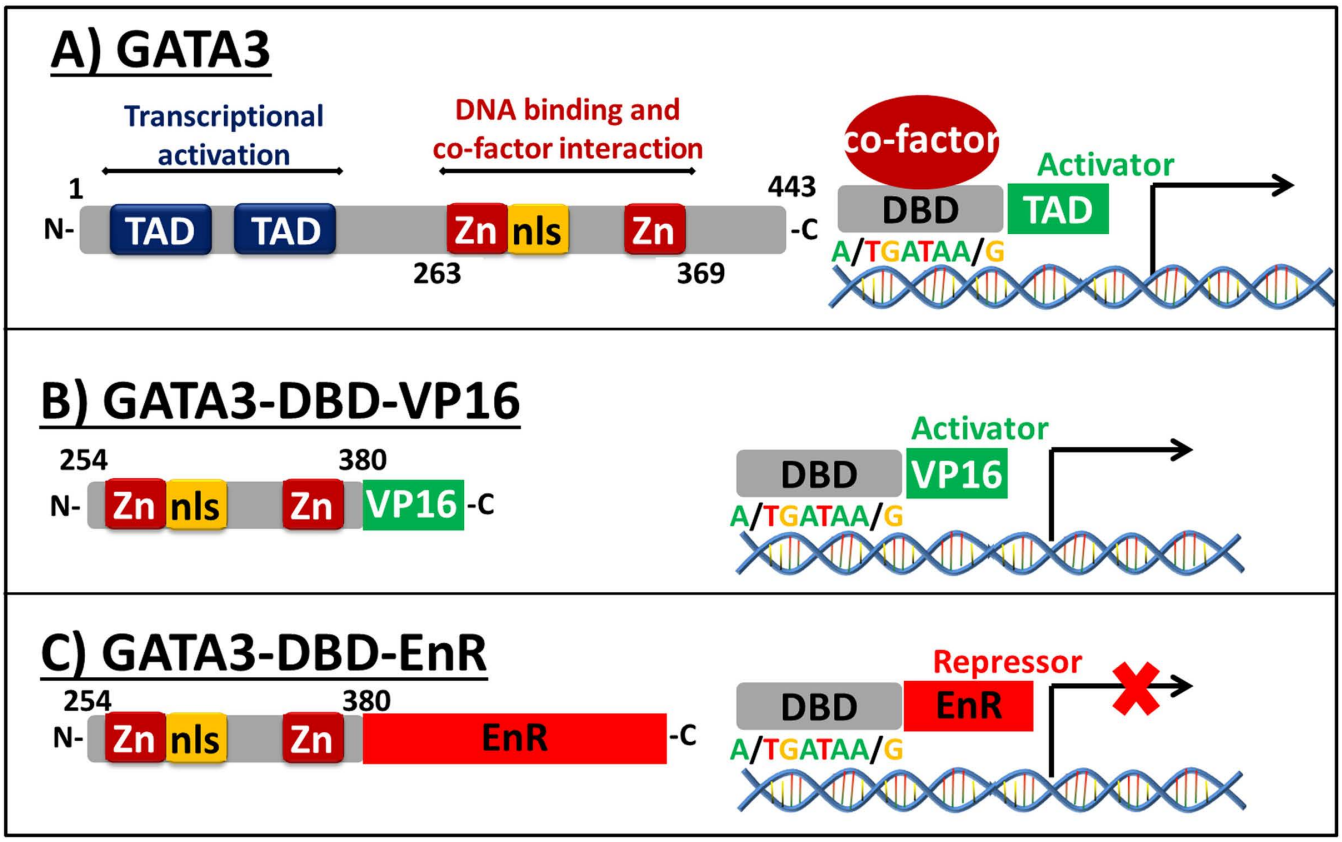

Fig. S4. Strategy adopted for generation of Gata3 gain-of-function and loss-of-function constructs. (A) Represents a full length mouse-GATA3 protein comprising of two amino-terminal transactivation domains followed by two zinc finger domains. (B) GATA3-DBD-V16 represents a constitutively active form of GATA3 generated by fusion of an in-frame strong trans-activator VP16 at the C-terminus of mGATA3 DNA binding domain. Thus constitutively transcribing the genes modulated by GATA3 binding. (C) GATA3-DBD-EnR represents a constitutively active form of GATA3 generated by fusion of an in-frame strong repressor EnR at the C-terminus of mGATA3 DNA binding domain. Thus constitutively repressing the genes modulated by GATA3 binding. The constructs were made as per method described by Kamei etet. al. (2011).

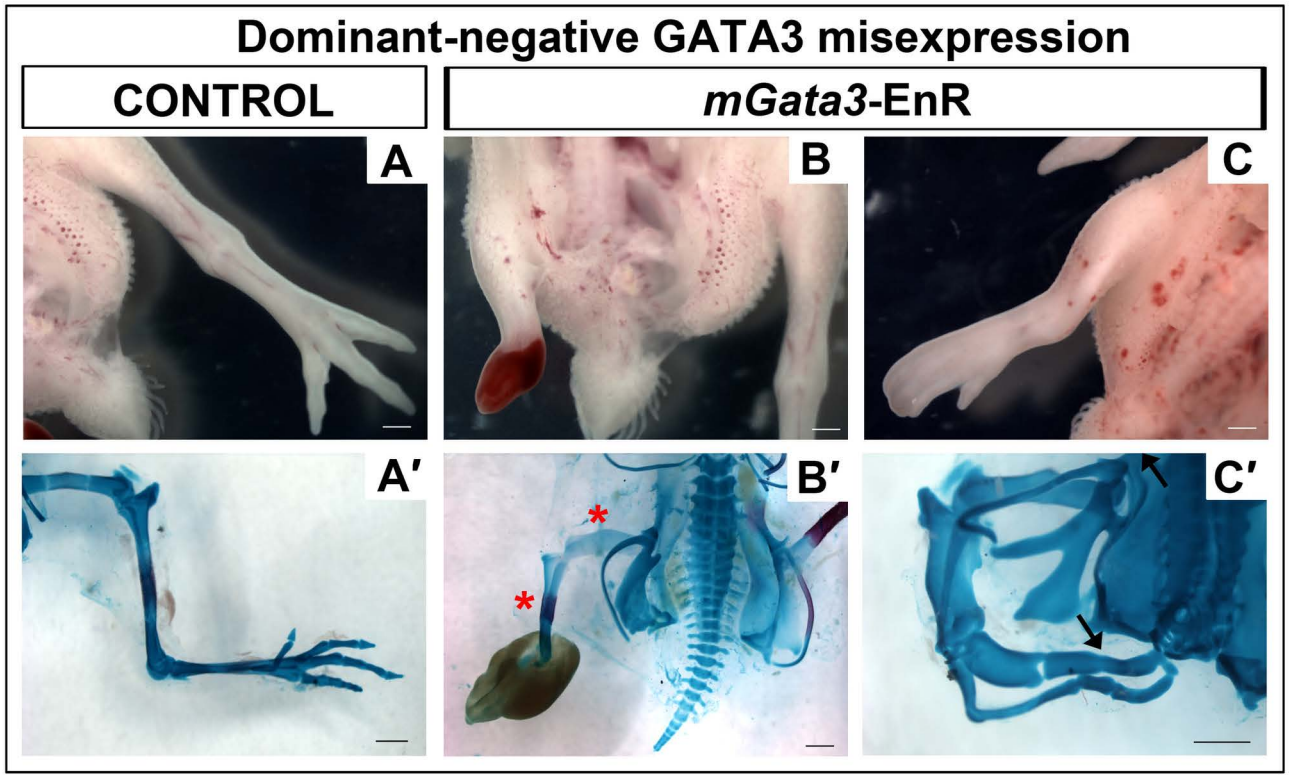

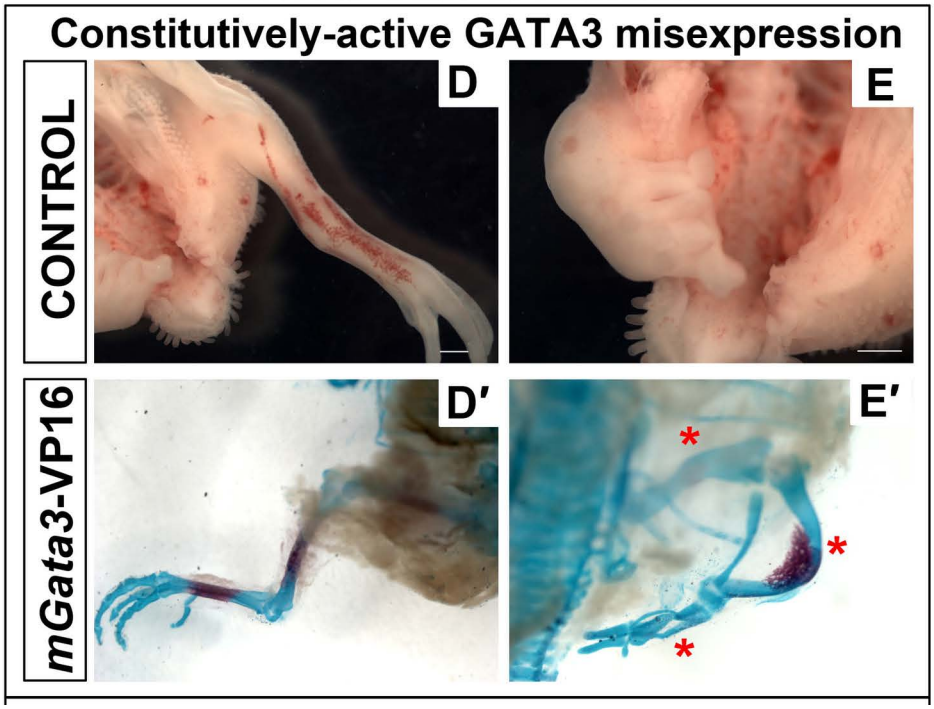

Fig. S5. *Gata3*-EnR and *Gata3*-VP16 infected limbs compared to respective uninfected contralateral control limbs. Whole mount view of unfixed, unstained RCAS-*Gata3*-EnR infected limb (B and C) and uninfected contralateral limb (A) at HH36. Alcian blue-alizarin red stained uninfected contralateral control limb (A′) and RCAS-*Gata3*-EnR infected limb with severe (B′) to less severe (C′) skeletal deformity. Arrows mark the unsegmented skeletal elements; red asterisks mark the elements showing reduced alizarin red staining. Whole mount view of unfixed, unstained RCAS-*Gata3*-VP16 infected limb (E) and uninfected contralateral limb (D) at HH36. Alcian blue-alizarin red stained whole mount skeletons from (D′) uninfected contralateral control limb and (E′) RCAS-*Gata3*-VP16 infected limb, where red asterisks mark the elements showing reduced alizarin red staining. Scale bar- 1mm.

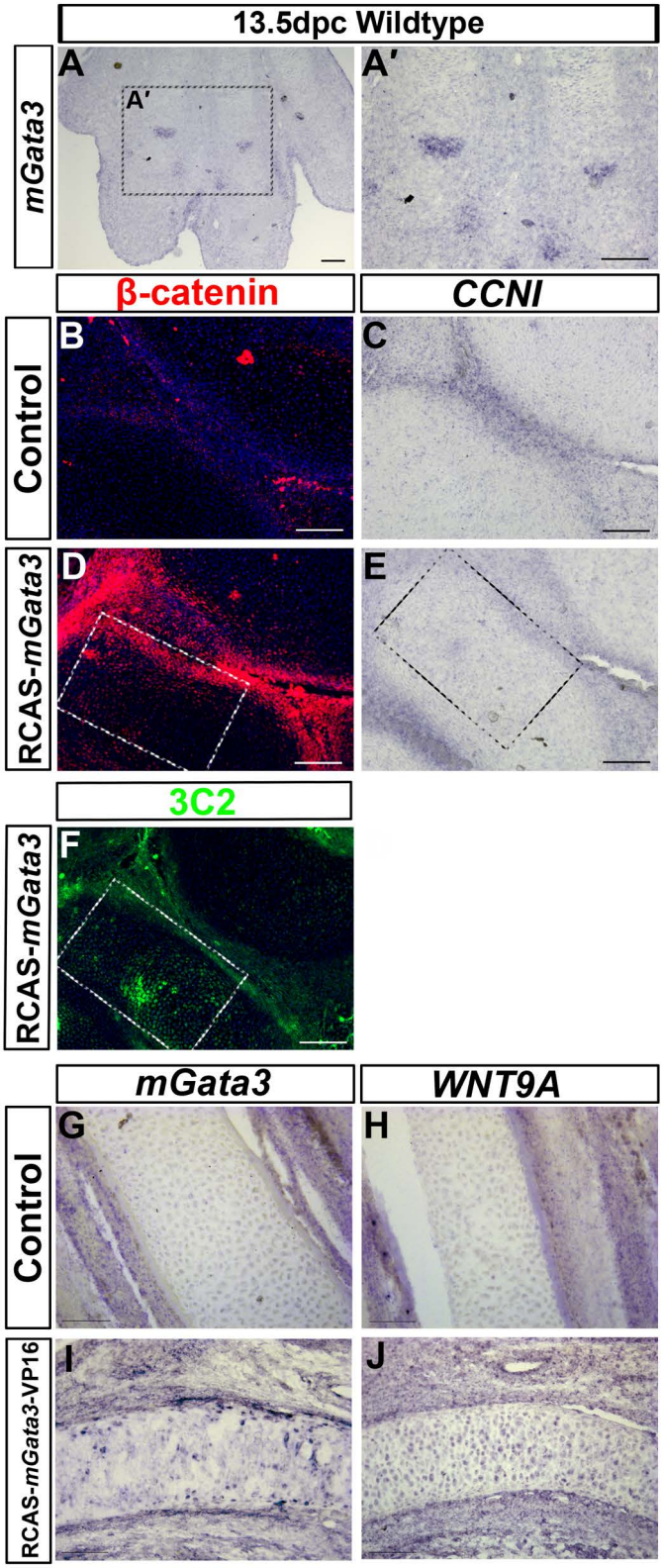

Fig. S6. Gata3 gain-of-function. (A) Expression of mouse *Gata3* mRNA in 13.5dpc mouse hindlimb digits. (A′) Magnified view of the boxed region in Panel A. (B-F) CCNI, an articular cartilage specific gene, is not overexpressed when mGata3 is virally misexpressed. (B and C) represent endogenous level of β-catenin immuno-reactivity (B) and CCNI mRNA expression (C) in tibio-tarsal joint of an uninfected contralateral control chick limb. (D and E) β-catenin immuno-reactivity (D), and CCNI mRNA expression (E), in the RCAS-m*Gata3*-cDNA infected HH36 tibio-tarsal joint region. (F) Immunohistochemistry with 3C2 (antibody against the viral gag protein) on a section serial to the ones used in panels D and E marks the viral infection domain in green within the boxed region. (G-J) Overexpression of mGata3-VP16 causes ectopic expression of Wnt9a. (G) RNA *in situ* hybridization against *mGata3* in non-infected contralateral control tibia. (H) RNA *in situ* hybridization against *WNT9A* in non-infected contralateral control tibia. (I) RNA *in situ* hybridization against mGata3 highlights the mGata3-VP16 infected tibia. (J) Ectopic expression of Wnt9a in the mGata3-VP16 infected tibia. I and J are serial sections. Scale bar- 100 µm.

Table S1: Articular cartilage specific genes that were identified as transcriptional targets of Gata3 in the microarray profiling performed by Kourous-Mehr et al. (2006).

ID_REF	VALUE	Avalue	Description	Symbol
22436	3.019	9.499	ectonucleotide pyrophosphatase/phosphodiesterase 2 (Atx)	Enpp2
36565	1.904	9.611	cyclin I	CCNI
11991	1.364	8.416	hypoxia inducible factor 1, alpha subunit	HIF1A
29726	1.112	9.046	cadherin 11	CDH11
14359	0.889	10.04	fibulin 1	FBLN1
18280	0.685	8.686	tenascin C	TNC
7418	0.412	12.638	growth differentiation factor 5	GDF5
13997	0.384	9.399	chordin	CHRD
12648	0.356	15.331	insulin-like growth factor binding protein 4	IGFBP4
12398	0.351	11.785	wingless-type MMTV integration site 9A	Wnt9a
31109	0.268	10.412	secreted frizzled-related sequence protein 2	SFRP2
27708	0.226	15.643	clusterin	CLU
13437	0.214	11.113	chondroitin sulfate proteoglycan 2 (versican)	CSPG2
35186	0.189	10.053	nuclear factor I/A	NFIA
14761	0.07	8.062	GLI-Kruppel family member GLI3	GLI3
8289	0.016	12.726	catenin (cadherin associated protein), beta 1, 88kDa	CTNNB1

#ID_REF = Unique Identifier
#VALUE = Lowess M Log Ratio (F635 Median, F532 Median), $\log_2$(Het /Null) where Het = fluorescence intensity of WAP-rtTA-Cre;GATA-3$^{flox/+}$sample and Null = fluorescence intensity of WAP-rtTA-Cre;GATA-3$^{flox/flox}$ sample
#Avalue = Lowess A Log Ratio (F635 Median, F532 Median)

Supplementary Table 2: List of clones used

Genes	**ChEST ID/ Source**
SFRP2	ChEST712d9
Atx	ChEST520a5
c-Jun	ChEST520g15
ERG	Cloned
PTHRP	Minina et al., 2001
NFIA *Nuclear factor I/A*	ChEST864l9
mNFIA	Deneen et al., 2006
mNFIX	IRAV 3491917
mGATA3	Kamei et al.,2011
PHLDA2 *Pleckstrin homology-like domain, family A, member 2*	ChEST533e11
Finished cDNA clone ChEST302p20	ChEST302p20
CCNI *Cyclin I*	ChEST605d20
GDF5	Hartmann et al., 2001
BMP4	Francis et al., 1994
COL2A1	Hartmann et al., 2001

mCOL2A1	
WNT9a	ChEST592n13
GATA3	ChEST663o17
IHH	Minina et al., 2001
PTHrPR	Minina et al., 2001

Hartmann C, Tabin CJ. 2001. Wnt-14 plays a pivotal role in inducing synovial joint formation in the developing appendicular skeleton. Cell 104:341-351.

Minina E, Wenzel HM, Kreschel C, Karp S, Gaffield W, McMahon AP, Vortkamp A. 2001. BMP and Ihh/PTHrP signaling interact to coordinate chondrocyte proliferation and differentiation. Development 128:4523-4534.

Kamei, C. N., Kempf, H., Yelin, R., Daoud, G., James, R. G., Lassar, A. B., Tabin, C. J., and Schultheiss, T. M. (2011). Promotion of avian endothelial cell differentiation by GATA transcription factors. Dev Biol *353*, 29-37.

Deneen, B., Ho, R., Lukaszewicz, A., Hochstim, C. J., Gronostajski, R. M., and Anderson, D. J. (2006). The transcription factor NFIA controls the onset of gliogenesis in the developing spinal cord. Neuron *52*, 953-968.

Francis PH, Richardson MK, Brickell PM, Tickle C. 1994. Bone morphogenetic proteins and a signalling pathway that controls patterning in the developing chick limb. Development 120:209-218.